Magnetic Field Measurements in the Electron Cooling Device for LEAR

A. Wolf, L. Hütten, H. Poth
Institut für Kernphysik

Kernforschungszentrum Karlsruhe

KERNFORSCHUNGSZENTRUM KARLSRUHE

Institut für Kernphysik

KfK 3718

MAGNETIC FIELD MEASUREMENTS

IN THE ELECTRON COOLING DEVICE FOR LEAR

A. Wolf, L. Hütten and H. Poth

MAGNETIC FIELD MEASUREMENTS

IN THE ELECTRON COOLING DEVICE FOR LEAR

A. Wolf, L. Hütten and H. Poth

Visitors at CERN from

Kernforschungszentrum Karlsruhe, Institut für Kernphysik

Fed. Rep. Germany

ABSTRACT

The field of the solenoid magnet to be used in the electron cooling device for LEAR has been investigated by careful field mapping. The magnetic field guiding the electron beam was measured in a volume with a cross-section of 6×6 cm^2 around the electron beam axis, which is 4.5 m long and bent twice in toroidal sections. A Hall-plate field scanner designed for the mapping of dipole magnets was used to obtain separate field maps of all Cartesian field components in rectangular boxes covering the aforementioned measuring region. For merging these maps into a consistent overall field table, an evaluation procedure has been developed that includes careful survey and the correction of errors inherent in Hall-probe measurements. The measured data are presented in plots of field components and of field lines, and the magnetic field properties of the electron cooling device are discussed. A short description of the computer programs produced during this work is also given.

Magnetfeldmessungen in der Elektronenkühlapparatur

für LEAR

ZUSAMMENFASSUNG

Das Feld des Solenoidmagneten, der in der Elektronenkühlapparatur
für LEAR verwendet werden soll, wurde durch sorgfältige Messung
einer Feldkarte untersucht. Das Führungsfeld für den Elektronenstrahl
wurde vermessen in einem Volumen mit 6 x 6 cm^2 Querschnitt um die
Elektronenstrahlachse, die 4,5 m lang ist und zwei Biegungen in
toroidalen Abschnitten aufweist. Ein mit Hall-Sonden ausgestatteter
Feld-Scanner, konstruiert für die Vermessung von Dipolmagneten,
wurde verwendet, um getrennte Feldkarten aller Cartesischen Feld-
komponenten in quaderförmigen Teilbereichen zu gewinnen, die die
erwähnte Meßregion überdecken. Damit diese Feldkurven zu einer
konsistenten Feldtabelle für den gesamten Bereich zusammengefaßt
werden können, wurde ein Auswerteverfahren entwickelt, das eine
sorgfältige geometrische Vermessung und die Korrektur der
charakteristischen Fehler von Messungen mit Hall-Sonden einschließt.
Die Meßergebnisse werden in Form von Feldkomponenten- und Feldlinien-
Diagrammen dargestellt, und die Magnetfeldeigenschaften der Elektronen-
kühlapparatur werden erörtert. Außerdem wird eine kurze Beschreibung
der Rechnerprogramme gegeben, die im Verlauf dieser Arbeiten erstellt
wurden.

Table of Contents

1. PURPOSE AND SCOPE OF THE MEASUREMENTS

1.1 The electron cooling magnet

The common technique to generate the intense electron flow for electron cooling of stored ion beams makes use of a magnetic field in the direction of the electron beam. This longitudinal magnetic field prevents the electron beam from blowing up owing to its space charge. The field strength is chosen in order to obtain a value of the electron cyclotron frequency which is large compared to the plasma frequency of the electron beam, and in order to match the requirements of the electron gun for producing a cold beam. The usually applied flux density is in the order of 1 kG.

The magnetic field influences the electron beam quality and the cooling performance of the device as explained in the following section. Therefore, the actual field properties should be optimized during the construction and operation of an electron cooling machine. On the other hand, the magnet geometry for electron cooling is quite complicated since it usually combines elements with different symmetries. The field lines are to follow the path of the electron beam which, apart from straight lines, also consists of curved segments for the electrons to enter and leave the vacuum chamber of the ion beam. Hence, solenoids and also toroid segments are present, which involves magnetic field measurements in the volume occupied by the electron beam. Incited by the specific case of the electron cooling device for LEAR[1], the present study demonstrates a systematic method to obtain reliable magnetic field data in the typical geometry of electron cooling magnets.

The assembly of magnets which is investigated is drawn in Fig. 1. The solenoids and toroids of the assembly are part of the magnet built for the electron cooling experiment performed at CERN within the ICE project[2]. The figure shows the path of the electron beam which is generated in the 1.3 m long *gun solenoid* and recovered by the collector attached to the end of the 0.7 m long *collector solenoid*. The toroidal magnets (*gun* and *collector toroid*) conduct the electron beam in and out of

the cooling region proper, situated in a third, 1.5 m solenoid *(cooling solenoid)*. Being only slightly deflected by the electron cooling magnet, the ion beam enters and leaves the cooling solenoid by passing almost straight through the toroids.

The assembly has one plane of (approximate) symmetry, parallel to the drawing plane of Fig. 1. Close to this symmetry plane, the magnetic field component perpendicular to it will be small compared to the longitudinal field strength. The symmetry is distorted by (a) the arrangement of the coil windings, and (b) manufacturing and assembly errors, to be detected by the measurements. The solenoidal and toroidal coils are surrounded by a soft iron screening tube that renders the field inside the coils independent of the magnetic environment of the device. The openings of the magnet can be covered by iron plates ("magnetic shunts"), leaving gaps only where necessary to operate the cooling device. Field inhomogeneities caused by the termination of the coils then extend into the magnet over a length approximately given by the dimensions of these small holes, only. At the collector end, a cylindrically symmetric iron configuration is used to shape the decrease of the axial field. During the magnetic measurements, all such additional iron parts were mounted. For the measurements, however, it was necessary to slightly enlarge the opening at the end of the gun solenoid.

Solenoids and toroids are bolted together at iron flanges in relative positions defined by dowel pins. Owing to the interruption of the coil, the longitudinal field strength in the magnet is slightly reduced near these flanges. In order to compensate this discontinuity, correction coils are mounted on the flanges of the cooling solenoid *(end-effect coils)*. They locally produce a longitudinal field of about 5% of the solenoid field.

Solenoids, toroids, and end-effect coils are connected in series to the same power supply. The correct fraction of the current passing through the end-effect coils is set by adjusting shunt resistors connected in parallel to them, and found with the help of the field measurements. Other shunt resistors bypass one coil layer of the toroids; they are adjusted in a similar way in order to match solenoid and toroid fields. This field trimming is described in Section 3.1.

For the operation of the cooling device other, small correction coils, producing transverse fields approximately homogeneous over the electron beam, will be used inside the magnet. They can change the field direction in order to steer the beam or to counteract variations of the field angle along the beam. These coils were not mounted during the measurements.

Finally, the reader is referred to Table 1 and Fig. 2 for more detailed information on dimensions and other characteristics of the magnet.

1.2 Objectives of magnetic measurements

The magnetic field properties are important for the operation of the electron cooler in the following respects:

i) The magnetic field lines determine the direction of the electron flow, and their curvature can excite the transverse motion of the electrons. Therefore, a tracking of the field lines and possibly of the motion of particles will be useful for optimizing the field. To provide data for such calculations, the field direction in a general reference frame should be determined with a precision of about 1 mrad; the position error accumulated in tracking a field line over 1 m would just be acceptable in this case ($\approx$ 1 mm). In particular, this precision should also be obtained in the inhomogeneous field of the toroids.

ii) In the cooling region where the electron and ion beams overlap, any variation of the magnetic field direction larger than about 5×10^{-5} rad deteriorates the cooling effect. This value can be estimated by observing that the cooling rate is limited by the larger value of either the relative electron velocity spread in longitudinal direction or the r.m.s. magnetic field angle[3]. In view of using small correction coils for straightening the field lines we hence want to measure field angle variations of the order of 0.05 mrad in the cooling solenoid (homogeneous field region).

These objectives call for the measurement of a field map in a volume around the nominal electron trajectory (see Fig. 1) large enough to cover the electron beam, 5 cm in diameter and 4.5 m long. The measuring probe must be adequate to determine all vector components of an inhomogeneous magnetic field. Alignment and positioning have to be controlled accurately and a large number of field values must be measured in a grid fine enough to obtain the field at any point by interpolation.

The magnetic measurement facility existing in the CERN EP Division has been employed for this purpose as far as it was useful. However, to reach the required precision and as a consequence of the particular geometry of the magnet, special procedures were necessary during the measurement and the data evaluation; these refinements will be described in Section 2.

2. MEASURING APPARATUS AND PROCEDURE

2.1 The scanning device

The device used for the field measurements is described in Section 3.1 of Runolfsson[4]. The probe head contains three Hall plates for measuring the Cartesian components of a magnetic field. It is fixed to the end of the *carrying arm*, a ceramic tube of about 2 m length which can be moved by the scanning device along three orthogonal axes. The apparatus with its scan axes i,j,k is shown in Fig. 3. The movement in the horizontal j direction corresponds to an axial displacement of the probe arm and has the largest scan range of 1.6 m.

For mapping the field of the electron cooling magnet, the scanner is moved to positions in which the j axis is aligned with one of the three solenoid axes. Several line scans parallel to these axes for different i and k coordinates allow the measurement of the magnetic field in rectangular volumes (measuring boxes). Since the j axis of the scanner must remain close to horizontal, for the measurement it is necessary to turn the magnet from its normal operating position by 90° around the cooling axis. Then, the symmetry plane of the magnet is horizontal, and the i and j axes of the scanner approximately lie in this plane.

The three Hall plates are mounted in the *probe head* as shown in Fig. 4. The normal vectors of the plates are oriented perpendicular to each other and can be aligned with the coordinate axes i,j,k by rotating the carrying arm and by adjusting two links. For the present measurements, a special probe holder was used (see Fig. 4) which allows the probe head to be mounted in different positions without new mechanical adjustment. Three plug-in mountings are available for displacements in the i direction and, in each position, the probe head can be mounted in two orientations rotated by 180° about the j axis. The advantages of this probe holder will become clear in the following sections.

The Magnetic Measurement Control System (MMCS)[5] allows one to control the scanner motion and the data taking with an on-line computer (HP1000). For fixed transverse coordinates, a line scan of the magnetic field components is performed by advancing the probe in the j direction and bringing the Hall plates to the same point in space one after the other, each time recording the Hall voltage. The data points are equally spaced along the measuring line. The results are written to magnetic tape, and the line scans are repeated for new equidistant i and k coordinates. The data points of a measuring box form a volume lattice. The spacings normally used in the present measurements are 20 mm in the j direction, and 10 mm in the i and k directions. Typically, 7 × 7 line scans were performed in the volume of one box (cross-section: 60 × 60 mm).

The MMCS also offers an off-line evaluation of the magnetic tapes, in which the Hall voltages are converted to values for the magnetic-field components. Independent calibration curves for the three Hall generators are used. The calibration is performed in a highly homogeneous field, using an NMR magnetometer[6].

The precision of the field maps obtained with this measuring system can be estimated from the mechanical and electrical properties summarized in Table 2. The resolution of the Hall voltage measurement and the stability of the measuring electronics are of the order of 10^{-4} for a magnetic field around 1 kG. Therefore, variations of the field direction by 0.1 mrad will be detectable, which is compatible with the requirements set up in Section 1.2.

In the inhomogeneous field of the toroid regions, the Hall-plate dimensions may limit the accuracy. The variation of the field direction over the Hall plate is given by the ratio of its size to the radius of curvature of the toroid magnet. Since this ratio is of the order of 10^{-3}, the error due to the Hall-plate size will not be larger than 1 mrad, as required.

If so far the precision of the measuring system appears satisfactory, other sources of error deserve special attention. Firstly, in view of their small dimensions, the orientation of the Hall plates is uncertain by about 10 mrad, even if the probe head is assembled and aligned very carefully. Secondly, large field components in the plane of the Hall generators will produce additional Hall voltages (transverse magnetoresistive effects) which do not appear during the calibration. For both reasons, the results of the standard evaluation cannot precisely be identified with the Cartesian field components B_i, B_j, B_k; only from a correction procedure, reliable values will be obtained.

2.2 Systematic errors and their correction

2.2.1 Transverse Hall effect

Hall generators are mainly sensitive to the magnetic field component along the normal vector of the probe plane ("normal" Hall effect). However, the field components in the probe plane can also influence the Hall voltage. For the Hall generators used in the present measurements, this transverse Hall effect is discussed in Ref. 4. With a planar field vector $\vec{B}_p$, the planar Hall voltage can be written

$$U_p = a_p IB_p^2 \sin \phi \cos \phi + a_T IB_{p,T}^2 + a_L IB_{p,L}^2 \ ,$$

where I is the Hall current and ϕ the angle between the current and $\vec{B}_p$; $B_{p,T}$, $B_{p,L}$ are the components of $\vec{B}_p$ perpendicular and parallel to the Hall current. The normal Hall voltage is written, with the normal field component B_n,

$$U_n = a_0 IB_n \ .$$

The first term in the expression of U_p represents the planar Hall effect with the coefficient given as[4]

$$a_p/a_0 = 0.38 \times 10^{-6} \ G^{-1} \ .$$

The other terms depend on the offset field value B_0 of the Hall plates used:

$$a_L/a_0 \approx 2 \times 10^{-10} \ G^{-1} \ (B_0/G)$$

$$a_T/a_0 \approx 3.5 \times 10^{-10} \ G^{-1} \ (B_0/G) \ .$$

Since the offset (i.e. the field measured with the screened probe) is of the order of 0.5 G in the present case, these terms can be neglected completely[*]. From the construction of the probe head, it follows that $\sin \phi \cos \phi$ vanishes for all Hall plates in the solenoid field regions, and no transverse Hall effect is expected there.

The situation is worse in the toroid field regions where, for the Hall plate measuring the vertical B_k component, a strong planar field with $\sin \phi \cos \phi \neq 0$ will occur. For 1 kG, the error of the vertical field angle as measured by this Hall plate will be of the order of 0.3 mrad and, therefore, affect the precision of the measurement.

Since the transverse Hall voltage is of second order in the components of $\vec{B}$ it can be distinguished from the normal Hall voltage by the fact that it does not change its sign if $\vec{B}$ is reversed. It has been decided to scan the magnetic field at both positive and negative values of the same magnet current. If the results at one point, obtained from the standard evaluation, are B_m^+ and B_m^-, where m = 1, 2, 3, the value retained for further use is

$$B_m = \left(B_m^+ - B_m^-\right)/2 \ . \tag{1}$$

In these results the transverse Hall voltage is supposed to cancel out.

---

[*] Much higher values of a_L/a_0 and a_T/a_0 are claimed in another paper[7], which are of the order of $0.1 \times 10^{-6} \ G^{-1}$.

2.2.2 Hall-plate misalignments

In order to take into account the exact orientation of the Hall plates, the components of their normal vectors $\vec{n}_m = (\alpha_m, \beta_m, \gamma_m)$ in the reference frame of the scanner (i,j,k) are considered. The results B_m, obtained from the separate conversion of Hall voltages *and* from Eq. (1), are the field components along $\vec{n}_m$. In the scanner reference frame, the result from plate m reads

$$B_m = \vec{n}_m \cdot \vec{B} = \alpha_m B_i + \beta_m B_j + \gamma_m B_k \quad (m = 1, 2, 3) . \tag{2}$$

If the direction cosines of the normal vectors are known, the components B_i, B_j, B_k can be calculated. (The final result is obtained by a coordinate transformation from the scanner reference frame to the magnet reference frame as described in Section 2.4.2.)

Owing to the particular construction of the probe head, and after its mechanical alignment with the scanner, the $\vec{n}_m$ deviate from the i, j, and k axes by small angles (< 10 mrad) only. Second and higher powers of these angles are therefore neglected. This implies that $|\alpha_1|$, $|\beta_2|$, and $|\gamma_3| \approx 1$ (error $< 5 \times 10^{-5}$). The other direction cosines can be directly identified with the small *misalignment angles* by which the plates deviate from their nominal orientations. For each plate, these angles correspond to certain rotations about the axes i, j, or k, according to Table 3.

Since the component B_k is perpendicular to the symmetry plane of the magnet, terms with misalignment angles γ_2, γ_3 are neglected altogether, being of minor importance as compared to other corrections. The field components in the coordinate frame of the scanner, corrected for probe misalignment to first order, are then obtained as

$$B_i = s_1(B_1 - \beta_1 s_2 B_2) , \qquad s_1 = \text{sign}(\alpha_1) ;$$

$$B_j = s_2(B_2 - \alpha_2 s_1 B_1) , \qquad s_2 = \text{sign}(\beta_2) ; \tag{3}$$

$$B_k = s_3(B_3 - \alpha_3 s_1 B_1 - \beta_3 s_2 B_2) , \qquad s_3 = \text{sign}(\gamma_3) .$$

It is seen that four Hall-plate angles are required for the correction procedure. Since the component B_j is large in the solenoids, β_1 and β_3 are most essential; α_3 and α_2 are of influence in the toroids only, where also B_i can be large.

Misalignment of the Hall plates is caused both by their mounting in the probe head and by the fixation of the probe head itself to the ceramic carrying tube. Therefore, it is necessary to know the actual orientation of the probe head during each scan with the accuracy which is required for the determination of the magnetic field direction. On the other hand, the relative orientation of the Hall plates within the probe may be determined once and for all in a separate measurement.

2.2.3 Determination of the Hall-plate directions

In certain field geometries, the Hall-plate misalignment angles can be determined by comparing measurements with different orientations of the probe head in the same field. Three different procedures are applied, which are based on this principle and will be described later in this section. With the exception of α_3, the misalignment angles are determined only once, with respect to a reference axis of the probe head itself.

To define this axis, a mirror of high optical quality is glued onto the front surface of the probe head (M in Fig. 4). Similarly to the Hall generators, it is mounted with high mechanical precision, so that the mirror plane is perpendicular to the probe head axis within 10 mrad. Before and after each volume scan, the orientation of the mirror surface is measured by *autocollimation*[8] with the same theodolite as that used to align the scanning device (see Section 2.4).

In this way, small angular deviations α, γ of the mirror normal $\vec{n} = (\alpha, \beta, \gamma)$ from the j axis can be measured with an accuracy of at least ± 0.05 mrad. The angles α and γ correspond to right-handed rotations about the negative k axis and the positive i axis, respectively. They are combined with *internal plate angles* $\hat{\alpha}_m$, $\hat{\beta}_m$ to obtain the Hall-plate directions

$$\beta_1 = \hat{\beta}_1 - s_1\alpha \ ,$$

$$\alpha_2 = \hat{\alpha}_2 + s_2\alpha \ , \tag{4}$$

$$\beta_3 = \hat{\beta}_3 - s_3\gamma \ .$$

The signs follow from the sense of rotation for each Hall plate angle as given in Table 3, and from the rotational axes for α and γ as mentioned above.

To find the internal plate angles, referring to the probe head axis as defined by the mirror, the misalignment of the single Hall plates must be determined together with the orientation of the probe head. The methods to find the misalignment are different for the β angles and for α_2, as illustrated in Fig. 5 and described below under (a) and (b). Further, since α_3 corresponds to a rotation about the j axis, which cannot be controlled by autocollimation during the measurement, a third method (c) must be applied in this case.

a)   Determination of β_1 and β_3

For a number of points inside the solenoid, the field components are measured twice; first the probe head is mounted in its normal position; then it is mounted in a position rotated about the j axis by 180°. The plug-in mountings in the probe holder assure the alignment of the probe with the scanner axes within 10 mrad in both positions. In addition, the probe orientation in both positions is measured by autocollimation. The comparison of the field values allows one to determine the internal plate angles $\hat{\beta}_1$ and $\hat{\beta}_2$ by the following method.

The Hall-plate signs are $s_1 = s_2 = s_3 = +1$ in the normal position ($\uparrow$), and $s_1 = s_3 = -1$, $s_2 = +1$ in the rotated position ($\downarrow$). From Eq.(3), neglecting products $\alpha_m B_i$ since B_i is small in the solenoid, and expressing the β_m by internal plate angles [(Eq. (4)], we find

$$\hat{\beta}_1 = \frac{B_1^{\uparrow} + B_1^{\downarrow}}{2B_2} + \frac{\alpha^{\uparrow} - \alpha^{\downarrow}}{2} \ ,$$

$$\hat{\beta}_3 = \frac{B_3^{\uparrow} + B_3^{\downarrow}}{2B_2} + \frac{\gamma^{\uparrow} - \gamma^{\downarrow}}{2} \ . \tag{5}$$

Note that, for accurate results, the probe must be rotated about a well-defined axis which, in this case, is measured by autocollimation.

b)   Determination of α_2

In order to determine the internal probe angle $\hat{\alpha}_2$ by a method similar to the one described in (a), it is necessary to orient the main field component along the

i axis and to rotate the probe head about this axis. Under these circumstances (Fig. 5b) access for the autocollimation measurement is available only if the main field is produced by a dipole magnet. A large dipole magnet of about $1 \times 0.5 \times 0.3$ m^3 field volume could be used. The well-defined rotational axis is provided by a large (30 cm diameter) turntable levelled horizontally within 0.05 mrad. The probe is mounted on the turntable as shown in Fig. 5b. Measuring components B_2 before and after a rotation by 180° (indicated by $\leftarrow$ or $\rightarrow$), the orientation of plate 2 with respect to the horizontal axis is obtained; it is given by $[B_2^{(\rightarrow)} + B_2^{(\leftarrow)}]/(2B_1)$. To find the internal plate angle $\hat{\alpha}_2$ suitable for later use, the angle α' of the mirror from the horizontal is measured by autocollimation and subtracted:

$$\hat{\alpha}_2 = \frac{B_2^{(\rightarrow)} + B_2^{(\leftarrow)}}{2B_1} - \alpha' . \tag{6}$$

c)   *Determination of α_3*

There seems to be no practical way to determine also α_3 by means of survey methods during the measurements and by an independent measurement of the internal plate angle. The value of α_3 can, however, be derived from the scan results themselves, using field values measured in overlapping scan volumes. This method takes advantage of the fact that the displacements of the scanner can be surveyed with high accuracy. It has only to be ensured that the probe head remains mounted on the carrying arm and is not moved relative to the scanner between the two scans.

Overlapping scan volumes in the toroids occur as a by-product in the measurement procedure (see Section 2.4). The first measurement (1) is taken on the cooling axis, the second (2) on the gun and collector axis, respectively. Between the measurements, the scanner is rotated about the previous k axis by a large angle θ ($\approx 36°$) and by small angles ϵ, δ about the other axes. With the transformation given in Appendix 1, the normal vector $\vec{n}_3^{(2)}$ of plate 3 after this rotation is obtained from the original one $\vec{n}_3^{(1)} = (\alpha_3, \beta_3, s_3)$. The two equations giving $B_3^{(1)}$ and $B_3^{(2)}$ [see Eq. (2)] can be solved for α_3 by eliminating B_k, yielding to first order:

$$\alpha_3^{(1)} = \left\{ B_3^{(1)} - B_3^{(2)} + s_1 B_1^{(1)} \left[s_3\delta \cos\theta - \left(\beta_3^{(2)} - s_3\epsilon \right) \sin\theta \right] + \right.$$

$$\left. + s_2 B_2^{(1)} \left[s_3\delta \sin\theta + \left(\beta_3^{(2)} - s_3\epsilon \right) \cos\theta - \beta_3^{(1)} \right] \right\} \Bigg/$$

$$\Bigg/ \left[s_1 B_1^{(1)} (1 - \cos\theta) - s_2 B_2^{(1)} \sin\theta \right]$$

$$\alpha_3^{(2)} = \alpha_3^{(1)} + s_3\delta .$$

(7)

In the case of the vertical field component B_k, agreement between results in over-lapping measurement volumes is forced at one point by fixing α_3 accordingly. It should be noted that at other points or for other components, the agreement of results in overlap volumes continues to provide an independent check of the accuracy of the correction procedure.

2.3 Mechanical preparations

2.3.1 Test for deformations of the magnet

Figure 6 shows the ground plan of the measuring site. The magnet is brought into its measuring position by turning it about the axis of the cooling solenoid which is supported by a cradle. During the rotation and in the measuring position, the weight of the gun solenoid must, in addition, be supported at some point off the cooling axis (usually P_1 in Fig. 6). By changing the height of this support, the orientation of the gun and collector axes is adjusted.

The validity of the measurements depends on the assumption that the magnet assembly can be considered as rigid. For the iron screening tube of 15 mm wall thickness, very small elastic deformations are calculated under the influence of the copper and steel weight: the sag of the gun solenoid, suspended horizontally at the toroid flange, amounts to 0.02 mm at the free end. Nevertheless the rigidity was tested. An attempt was made to measure deformations that might occur when the positions of additional supports off the cooling axis are changed.

With a theodolite, six reference points in one vertical plane were defined on the magnet flanges for the test when the magnet was still vertical. After rotation, the distances of the same points from the horizontal plane were measured optically. In the case where the magnet moves rigidly, it should be possible to

fit a plane to the coordinates of the points; deviations from a fitted plane will indicate deformations of the magnet. The deviations found are shown in Fig. 7 for different arrangements of the supports. In view of the estimated measuring error of ±0.1 mm, the deviations and, in particular, their correlation with the arrangement of supports are not significant.

2.3.2 Definition and survey of reference points and axes

Reference marks on the magnet axes allow one to specify the coordinates of points within the magnet, and to relate them to scanner coordinates. The reference marks are realized by cross-wire survey targets mounted in removable aluminium bars on the magnet flanges. They define the three axes P_1Q_1, P_2P_3, P_4Q_4 (see Fig. 6) to which the scanning device is aligned for the measurement. P_1 to P_4 serve as starting points on the measuring axes, in order to define the origin of the scanner coordinates.

The axis P_2P_3 coincides well with the mechanical axis of the cooling solenoid coil; the estimated deviation of P_2 and P_3 from the mechanical axis is some tenths of a mm. The other targets are related to the mechanical axes of the gun or collector solenoid with larger tolerances.

The determination of the target coordinates and axial directions was done by a survey team. Target coordinates are known to ±0.3 mm, and the angles between axes to ±0.05 mrad. The survey results are summarized in Table 4. They refer to the notation of angles specified in Appendix 1, and to rectangular coordinate axes xyz (magnet frame) defined as follows:

origin : P_2,

y axis : P_2P_3,

x axis : horizontal in the measuring position, pointing away from the gun

solenoid.

The rotational position of the magnet about the y axis remained fixed during the measurements. It was so chosen in order to have minimal deviations of the gun axis P_1Q_1 and of the collector axis P_4Q_4 from the horizontal plane. The orientation

of reference planes on the gun-side flange of the cooling solenoid is given in
Table 4, so that the direction of the x axis can be reproduced.

2.4 Production of the field map

2.4.1 Disposition of measuring boxes

During all the measurements a magnet current of 800 A corresponding to a lon-
gitudinal field of approximately 1220 G was set. Volume scans are performed in ten
measuring boxes numbered in the sequence in which the measurements are taken (see
Fig. 1). Figure 6 indicates the four positions of the scanning device.

The volume in which the electron beam travels is almost completely covered by
four long scan volumes centred on the three axes (Boxes 1,3,5,7). In the toroids,
additional regions cover the remaining beam volume (Boxes 2,4,6,8).

The field map is continued into the collector (Box 9) and along the proton
beam on the collector side of the cooling axis (Box 10). The original iron confi-
guration at the collector (see Fig. 1) was mounted for scanning Box 9, but not
for Box 7, where the hole in the magnetic shunt was larger. Results from the
collector region are discussed separately in Section 3.4.

The currents in the third coil layer of the toroids and in the end-effect coils
were adjusted before the scan of Box 1 at the gun toroid, and before the scan of
Box 5 at the collector toroid. Before measuring Box 1, the effect of the adjustment
at the collector toroid on the field in Box 1 was tested. The probe head was moved
into the cooling solenoid as deep as possible (about 1 m from the gun solenoid
flange); no field variations were detectable when the currents at the collector
toroid were changed. The adjustment and the properties of the field in the toroids
are discussed in more detail in Section 3.1.

2.4.2 Coordination of volume scans

The results of each measuring box refer to the axes i, j, k of the scanning
device. The coordinates of the measuring points are given by

$$i = (n_i - 1) \Delta i, \quad j = (n_j - 1) \Delta j, \quad k = (n_k - 1) \Delta k , \tag{8}$$

where Δi, ..., Δk are the point spacings, and n_i, ..., n_k are integer numbers, which are the indices of the three-dimensional table in which the results are stored ($n_i = 1$, ..., N_i, etc.). The origin thus corresponds to the first data point in the table.

Three angles θ, ε, δ are used to describe the orientation of each ijk frame in the general xyz frame. The angle θ describes the orientation of the j axis in the horizontal xy plane (azimuth), ε the deviation of the j axis from this plane (pitch), and δ the deviation of the i axis from this plane (roll). The coordinate transformation is given in terms of these angles in Appendix 1.

The complete data of the field map consist of ten tables for the measuring boxes, each accompanied by the parameters defining the box reference frame. In this form, the field map is available as a random access file on the CDC computer system at CERN. Details of the programs used to generate the field map and to present the results can be found in Appendix 2. The box parameters are summarized in Table 5.

In the following, the survey procedure used to obtain these parameters is described. The j axis of the scanning device is surveyed relative to the target axes using a theodolite. The horizontal circle of the theodolite corresponds to the azimuth θ, the vertical circle to the pitch ε. The theodolite is installed opposite to the scanning device, facing the probe head. First, it is aligned with the front and rear cross-wire targets. Then the targets can be removed to allow the scanner to be put into place. The centre of the probe head (marked by a cross on the front mirror) is observed during a scan in the j direction. By adjusting azimuth and pitch, the alignment of the scanner is improved; finally, the angles under which the probe centre appears at the front and rear positions of the j scan are read on the theodolite. The complete survey data consist of eight theodolite readings, namely horizontal and vertical angles for rear and front targets and rear and front probe head centres. From these values, the horizontal and vertical angles between the target axis and the scanner axis are calculated using the construction shown in Fig. 8.

From the same theodolite position, autocollimation of the probe head mirror is also performed, so that the angle between scanner axis and mirror normal can be calculated.

The roll angle δ, finally, is specified by levelling the rails that define the i axis of the scanner into a horizontal position. For all the measurements mentioned, a precision of ± 0.05 mrad is estimated.

3. RESULTS

3.1 Field trimming at the solenoid-toroid transitions

In this section, the results of the current adjustment for the toroids and end-effect coils are presented. The aim was to obtain a constant field strength on the electron beam axis in the toroids and solenoids.

As a criterion for the adjustment, the y component of the magnetic field on the y axis of the magnet (cooling axis) was measured. In the toroid, this measuring line deviates fom the electron beam axis but it is possible to determine the field strength on the bent electron trajectory from the measured curve B_y $(0,y,0)$. For a constant field strength B_0 along the electron beam, the field behaviour will be approximately given by

$$B_y(0,y,0) = \begin{cases} B_0 & \text{(in the cooling solenoid)} \\ \\ B_0/\left[1 + (y - y_T)^2/R^2\right] & \text{(in the toroid)} \end{cases} \tag{9}$$

where y_T is the coordinate at which the toroid starts, and R the toroid radius of curvature (Table 1). The derivation of the lower expression, considering the radial decrease of the field strength in the toroid, is explained by Fig. 9. The function given by Eq. (9) does not take into account the mutual influence of the solenoid and toroid magnets near the junction but only the individual field symmetries. In addition, the field strength will be reduced near the magnet flanges by the interruption of the coil.

Figure 10 shows the field behaviour measured during the adjustment at the gun solenoid. Firstly, the current in the end-effect coil is increased to compensate

the field depression (curves 1 to 3). Secondly, the current in the third layer of the toroid coil is increased in trying to obtain the field given by Eq. (9), see measured curves 4 to 6.

The field shape at both toroids after the adjustment is shown in Fig. 11; the adjusted current values are given in Table 6. The agreement that could be obtained between the measurement and Eq. (9) (calculating with the nominal values of y_T and R) is quite good at the gun toroid but worse at the collector toroid. Deviations from the nominal geometry, which would explain the observed disagreement, become obvious from the field line tracks discussed in Section 3.5.

3.2 Field dependence on the magnet current

A series of line scans for magnet currents between -1000 and 1000 A was made on the cooling axis, in the solenoid and the collector toroid (central line of Box 5). These measurements allow the determination of the proportion between current and longitudinal field strength, and the detection of unwanted effects of the iron screening caused by ferromagnetic phenomena. Although some indications for the latter effects are found in the data, no further time was spent during the measurements to study these phenomena in more detail since they appear to be of minor importance in any case.

Firstly, results from the centre of the cooling solenoid (y = 1504 mm, x = 0, z = 0) are presented. The B_y component as a function of the current is well fitted by a straight line. The residual deviations are plotted in Fig. 12. B_y was continuously changed from negative to positive values during the measurement. The offset field, which may be caused by iron magnetization, was -2.1 G, and the slope was 1.523(1) G/A. It is seen that the ambiguity introduced by ferromagnetic effects is of the order of ±2 G, at a maximum. The slope is 3% smaller than the theoretical value of 1.57 quoted in Table 1. This is probably due to the non-uniform current distribution in the coil (electrical insulation and water cooling channels).

In Fig. 13 the transverse components at the centre of the cooling solenoid are plotted against the magnet current. There is no regular non-linear behaviour

apparent and it can be concluded that the field direction does not depend on the field strength within the accuracy of the measurements (0.07 G).

In the toroid field, 500 mm from the start of the collector toroid (y = 2704, x = 0, z = 0), the situation is different. The component B_z versus the magnet current is shown in Fig. 14. The deviations from a straight line, fitted to points at low current, are regular and large compared to the experimental error. They may be decomposed into symmetrical and antisymmetrical contributions. Symmetrical contributions are expected from the planar Hall effect which of course is not suppressed in the measured data; it amounts to an error of 0.8 G at a field strength of 1.52 kG in good agreement with Section 2.2.1. After subtraction of these contributions, the values for B_z lie on the dashed curve in Fig. 14, with deviations from the straight line of ±1.5 G at ±1000 A. The B_x component shows no significant deviations from linear behaviour. A possible explanation for the trend of B_z is the following:

The current in the third, outer toroid coil layer passes through the iron screening only once, contrary to the currents in all other coils of the magnet which always enter and leave the iron screening at the same points, two coil layers with opposite pitch being connected in series. In connection with the toroid geometry, the current in the third coil layer obviously violates the mirror symmetry of the magnet about the x-y plane. Hence, a field component in the z direction is caused by this current. Indeed, B_z assumes values of the order of 10 G in the toroids, as compared to values of the order of 1 G in the solenoids.

The screening iron influences the field produced by the current I_T in the third coil layer (Fig. 15). In particular, image currents are effective for high relative permeability μ, and especially the image current I'_T appearing on the side towards the toroid bending centre will influence the field on the electron axis. If, for an estimation, one assumes the current to be concentrated near the electron axis, then the flux density B_z in the iron (at the point indicated in Fig. 15) will be $B_z = \mu\mu_0 I_T/(2\pi f) \approx \mu I_T \times 10$ G/kA (f = 0.2 m).

For large μ and I_T up to 0.5 kA, a high flux density is expected in the iron. This leads to a reduction of the permeability, so that, speaking in terms of image currents, their effect will be reduced, and the saturation-like behaviour as measured in Fig. 14 appears.

Quantitatively, the absolute value of the vertical field angle in the toroid decreases by 1 mrad, from 10.6 mrad, between 400 and 1000 A. On the other hand, the field angles in the solenoids are found constant within 0.1 mrad in the same current range. It can be concluded that no other saturation effects were observed and that hence the field map is valid for a wide range of longitudinal field-strength values.

3.3   The field map

3.3.1   Presentation of data

Listings and plots of the field components are obtained from the data tables (see Section 2.4.2) using a specially developed program, FPLOT. The field can be presented along straight lines of any direction in the magnet coordinate frame xyz. A system of rectangular axes, along which the field components are taken, can be defined freely. For equally spaced points along the defined line, the field components are found by interpolation between the adjacent measured values.

With a spacing of Δj = 20 mm between measuring points and the toroid radius R = 1050 mm, linear interpolation can lead to a field direction error of the order of $(\Delta j/R)^2 \approx 0.4$ mrad in the inhomogeneous toroid field regions. Therefore, quadratic interpolation is used instead to determine the field components at any point. Hence the error is reduced to the third power of the above ratio. For points in a selectable range outside the box volume, the field is found by extrapolation.

Results from all boxes in which the field can be interpolated are listed or plotted for each requested point. By implementing geometry-related subroutines, the requested points can be defined along curved trajectories, and the field components can be obtained in curvilinear reference frames. This feature is used to display the field components along the electron beam (Section 3.3.3).

3.3.2 Field on the cooling axis (ion trajectory)

The field components in the magnet frame along the line x = 0, z = 0 are shown in Fig. 16. In order to find the behaviour of the magnetic field all along the trajectory of the cooled ions, the measurement has been carried on through the collector toroid until the end of the magnet (Box 10). Assuming the same trend in both toroids, the components B_y and B_x in the gun toroid are also indicated in Fig. 16 by dashed lines.

In the toroids, the cooled ions are subjected to an important transverse field component B_x, reaching almost half the longitudinal field strength over a short length. The integral over B_x along the cooling axis determines to first order the deflection of the ions in the z direction. Its value for the collector toroid is found from the measurement to be

$$\int_{\substack{\text{collector} \\ \text{toroid}}} B_x \, dy = B_0 \times 0.234(1) \text{ m} .$$

It has been calculated from the sum over the interpolated points plotted in Fig. 16, using for B_0 the longitudinal field strength in the centre of the cooling solenoid (1220 G).

The action of the longitudinal field B_y on the cooled ions consists in rotating their transverse velocity vector about the y axis. The angle of this rotation during one passage of the cooler is obtained from the field integral over the component B_y. The measurement yields

$$\int_{\substack{\text{collector} \\ \text{toroid}}} B_y \, dy = B_0 \times 0.679(2) \text{ m} .$$

The total field integral of the longitudinal component is $B_0 \times 2.85$ m if the same field behaviour is assumed for the gun toroid.

The z component of the magnetic field shows variations in the cooling solenoid, which are discussed in the next section. In the toroids, B_z assumes higher values up to 10 G which presumably are a consequence of the current in the third toroid coil layer (see Section 3.2). In general, the magnetic field values found for the

same point in different measuring boxes, plotted separately in Fig. 16, are in good agreement. We conclude that systematic errors are avoided by the applied evaluation procedure.

3.3.3 Field along the electron beam

The magnetic field seen by the electron beam is most clearly presented in a frame in which the transverse coordinates are taken from the beam centre. To define this reference frame tsv, straight lines and circle segments are connected to a continuous curve in the xy plane describing the nominal electron trajectory (beam centre). For any point given, the s coordinate is the path length on this curve to the point on the curve closest to the given point. The transverse coordinates are the normal deviations from the curve in the xy plane (t coordinate) and in the vertical direction ($v \equiv z$), respectively. The transformation formulae for point coordinates and field components are collected in Appendix 3.

Figure 17 shows the behaviour of field components B_s, B_v, and B_t along the electron beam. The field is plotted for a trajectory on the nominal beam axis ($t = 0$, $v = 0$) and for paths diagonally displaced from this axis ($t = v = 20$ mm, $t = v = -20$ mm).

In the longitudinal component B_s, four major depressions appear, namely near the magnet ends (1, 4) and, because of missing coil turns, at the toroid junctions with the gun and collector solenoids (2, 3). Further, the longitudinal field in the toroids varies with the t coordinate which corresponds to the distance from the toroid bending centre.

The transverse components are mostly uniform over the electron beam cross-section, except for non-uniform distortions, depending on the t and v coordinates, in some regions (shaded areas in Fig. 17). The latter obviously are associated with longitudinal field variations, as at the toroid junctions. The measurement shows that, by the end-effect coils, such non-uniform transverse fields are to a large extent avoided in the cooling solenoid. Uniform field angle variations can be corrected quite easily using small dipole coils near the inner walls of the magnet tube, which produce homogeneous transverse fields.

It follows from the measurement that such correction will be necessary in the cooling solenoid to meet the requirements stated in Section 1.2. The strongest field angle variation occurs in the right hand part of the solenoid (s ≈ 1000 m). It probably can be explained by an irregularity in the iron screening tube of the cooling solenoid; measuring the vertical distance of the outer tube surface from a ruler placed approximately parallel to the magnet axis, the profile shown in Fig. 18 is obtained. Points scattering around straight lines represent the unmachined tube surface. Near s = 800 mm, material has been taken off by grinding; the vertical angles of the tube left and right of this region differ by 2.4 mrad. This indicates that two pieces of tube have been welded together. Similarly to the vertical field component, the tube angle is lower on the right side of the irregularity.

Since no sudden transition can be achieved between solenoid and toroid fields, the component B_t starts to increase already in the cooling solenoid, near the toroid junction, and the homogeneous field region is inevitably somewhat shorter than the cooling solenoid. The measurements show (see Fig. 17) that this end effect on the t component is smaller than 1 G at a distance of 100 mm from the solenoid end. Therefore, assuming that the field inside the solenoid can be rectified by dipole correction coils, an effective electron cooling length of approximately 1.3 m can be expected.

3.4 <u>Magnetic field at the collector entrance</u>

The decrease of the magnetic field at the collector entrance has been measured in Box 9 with the iron configuration to be used for operating the electron cooler (see Fig. 1). The comparison (Fig. 19) of the measurement with the results of a field calculation using the POISSON program[9] shows good agreement in the region of fast field decrease on the upstream side of the solenoid flange. Still inside the solenoid, some measured values lie slightly below the calculated curve, because the coil effectively terminates earlier than assumed in the calculations.

For the measurement of Box 7 (collector solenoid and toroid) the magnetic
shunt at the collector entrance was replaced by a simple Armco iron disk, which
is 15 mm thick and has an opening of 120 mm diameter instead of the 84 mm hole of
the magnetic shunt shown in Fig. 1. In spite of the larger diameter of the opening,
the field starts to decrease less rapidly with the provisional configuration.
In Fig. 17, near arrow 4, the values for B_s from Box 7 lie above those from Box 9.

3.5 Field line tracks

A second way of presenting the measurement results contained in the field
data tables is to display magnetic field lines. After leaving the gun, the elec-
trons follow the magnetic field lines if changes in the field direction occur
slowly compared to the cyclotron motion; thus the field line pattern represents
the drift motion of the electron beam in an adiabatic approximation, which is
approximately valid in the electron cooling device.

Strictly speaking, a magnetic field line should stand for an amount of magnetic
flux constant throughout the field line path, and the distance of the field or flux
lines in a field line pattern should signify the flux density, i.e. the magnetic
field strength. For the field line patterns derived in the present field line
tracks, however, the latter interpretation is not normally applicable. Only the
property that the field line tangent always has the direction of the flux density
vector is used: once a starting point has been defined, the trace of a single
field line is followed wherever measurement results are available. The starting
points for a bunch of field lines, on the other hand, can be defined deliberately
so that the distance between them need not have any significance.

Mathematically, the field line track is equivalent to finding a function of
the three space coordinates from a direction field. The direction field is defined
by the measured data tables in which quadratic interpolation is performed. The
field line is started with a third-order Runge-Kutta routine and continued with
a simple predictor-corrector method (Appendix 2). This had the advantage that an
error estimate is obtained. The averaged absolute value of the predictor-corrector
difference for the field line tracks performed is 10^{-4} of the step length, which
was always 12 mm.

A useful application of the field line tracks is to find the radius of curvature and the centre of curvature of field lines in the toroids. Both follow from the second derivatives of the coordinates with respect to the path length along the field line; a practical way to obtain the derivatives is to use a spline fit library routine (Appendix 2). The curvature of the field line started on the target-defined axis of the gun solenoid, near the cathode location, is plotted in Fig. 20; in particular, the plot gives an impression of the extension of the transition region between solenoid and toroid fields. The oscillations appearing in the figure are artefacts occurring when the field line passes from one data box into another; they are caused by the remaining small discrepancies between the results of different measuring boxes which locally disturb the spline fit results. The trend of the plotted values continues through the oscillations.

Figure 21 shows the instantaneous positions in the xy plane of the centre of curvature along a field line in the toroids. In the enlarged diagrams, the motion of the centre point as the field line enters and leaves the toroid can be seen (arrows). Inside the toroids, the centre coordinates lie within the circles marked by C_1 and C_2. For both toroids, the distance from the cooling axis (x coordinate) of the centre points is about 7 cm smaller than the nominal radius R (105 cm). The displacement from the nominal position in the y direction is about 2.5 cm on the gun side and about 5 cm on the collector side. Note that the symmetry of the toroid about the dash-dotted line in Fig. 21 seems to be considerably more disturbed on the collector than on the gun side: the arc of the field line is rotated counter-clockwise about the z axis in both cases, by 4° on the gun side but by 9° on the collector side.

The path of the field lines started at the cathode is finally shown in Fig. 22. The coordinates have been transformed into the frame accompanying the electron beam (see Section 3.3.3, Appendix 3). It is seen (arrows in Fig. 22) that the field line which started at the cathode centre is displaced by about 0.8 cm from the cooling axis and ends up with a displacement of about 1.5 cm at the collector entrance. Thus the field line track yields valuable hints for the steering of the beam by small transverse fields using correction coils.

4. SUMMARY AND CONCLUSION

A procedure was described to measure the field of a particular magnet configuration (solenoidal and toroidal sections) with high precision. Mechanical alignment methods, systematic field measurement errors and their corrections were studied in detail.

These procedures were applied to map the magnetic field of the electron cooling device for LEAR. It was demonstrated that the direction of the magnetic field could be determined with an absolute precision of the order of 0.1 mrad. This allowed for the combination of data from separately scanned volumes and in turn provided a field map of the whole region which will be traversed by the electron beam. Using this map, the trajectory of electrons can be traced through the cooler and the transverse heating during this motion can be determined.

The field map clearly shows that the field of the investigated magnet is not sufficiently regular when considering the high quality required. This is obvious in the cooling region as well as in the toroids. The field measurements, however, will allow us to design and install suitable correction coils which we expect to considerably reduce the transverse heating of the electrons, and to improve the cooling performance.

Table 1

Technical data of the magnet

	Symbol[a]	Solenoids	Toroids	End-effect coils	Unit
Coils					
Copper conductor size		15 by 15	15 by 15	4 by 4	mm
Water cooling channel diam.		10	10	2.5	mm
No. of coil layers	n_L	2	3	2	
Average winding radius	a	163	171.5	134	mm
Coil thickness	b	32	50	10	mm
Bending radius (axis)	R	∞	1050	∞	mm
Length (axis)	ℓ	1500,1300,700[b]	1050 × 0.2π = 660[c]	30	mm
Distance of winding centres[a]	c	0	266	0	mm
Inner radius (usable space)	d	142	142	129	mm
Winding density (per layer)	n_{eff}	62.5	62.5 × 0.813[d]	200	turns/m
Resistance[e]		14.5/m	11.7 (inner layers) 6.3 (outer layer)	17.9	mΩ
Field on axis (theory)		1.57[f]	1.92[f]	0.56[g]	G/A
Power[h]		14.5(58)/m	18(72)	0.41(1.65)	kW
Water cooling					
Water flow required[h,i]		0.12(0.48)/m	0.15(0.60)	0.0033(0.013)	ℓ/s
Cooling channel length		100[j]	36	11	m
Pressure drop[k]		1.8(20)[j]	0.23(2.6)	0.5(5.3)	kg/cm²
Screening tubes					
Iron thickness	e	15	15	–	mm
Outer dimensions	f	198	217	–	mm
Weight		345/m	380	–	kg

a) See Fig. 2

b) Cooling, gun, collector solenoid, respectively.

c) Bent axis, 36°.

d) Effective winding density on axis: reduction factor = (R - a - b/2)/R.

e) Coil layers connected in series; measured values.

f) $B/I = \mu_0 \, n_{eff} \, n_L$.

g) $B/I = \mu_0 \, n_{eff} \, n_L \, \ell/\sqrt{\ell^2 + 4a^2}$.

h) At 1000 (2000) A, 150 (300) A in end-effect coils.

i) Temperature rise 30°C.

j) 1,5 m solenoid.

k) Cooling channels in parallel, except end-effect coils.

Table 2

Characteristics of the magnetic measurement device

Scanner	
Axial scan range (j direction)	160 cm
Transverse scan ranges (i and k directions)	50 cm
Positioning accuracy	0.1 mm
Line scan speed (j direction)	1.3 cm/s
Probe head	
Length (j direction)	100 mm
Transverse size (i, k)	20 mm
Operating temperature	$(40 \pm 0.5)\,^\circ C$
Accuracy of alignment	10 mrad
Hall generators[4]	
Type	Siemens SBV579
Size of active area	1.6×1.6 mm^2
Sensitivity a_0	≈ 140 µV/(AG)
Temperature coefficient of a_0	$\approx -4 \times 10^{-4}/^\circ C$
Accuracy of alignment	10 mrad
Electronics	
Hall current	100 mA
Current supply type	Hewlett Packard 6181 C
Current variations	$\pm 5 \times 10^{-5}$
Current connections to Hall generators	in series
Hall voltage for 1 kG	≈ 14 mV
Integrating digital voltmeter type	Hewlett Packard 2402 A
resolution	1 µV
offset drift during 1 hour	≤ 1 µV

Table 3

Properties of small rotations and correction methods related to Hall-plate direction cosines α_m, β_m, γ_m

	α_2	α_3	β_1	β_3	γ_1	γ_2
Hall-plate number	2	3	1	3	1	2
Main component	$s_2 B_j$	$s_3 B_k$	$s_1 B_i$	$s_3 B_k$	$s_1 B_i$	$s_2 B_j$
Disturbing component	B_i	B_i	B_j	B_j	B_k	B_k
Axis of rotation	k	j	k	i	j	i
Sense of rotation[a]	$-s_2$	$+s_3$	$+s_1$	$-s_3$	$-s_1$	$+s_2$
Correction method	b	c	a	a	no correction	

a) Positive if main component, disturbing component, and axis of rotation form a right-handed coordinate frame in the sequence given. See Eq. (3) for s_1, s_2, s_3.

Table 4

Survey results for reference targets
and definition of the magnet coordinate frame

a) Reference point coordinates in mm

Point	x	y	z
P_1	-966.6(3)	-917.0(3)	5.45(10)
P_2 (origin)	0.0	0.0	0.0
P_3	0.0	3011.4(3)	0.0
P_4	612.9(3)	3444.7(3)	-0.79(10)

P_1 and P_4 are intersections of target-defined axes with the flange surfaces.

P_2 and P_3 are intersections of target-defined axes with machined reference planes of the target bars.

b) Axis angles in mrad

Axis	Azimuth	Pitch
P_1Q_1	-627.75(5)	-2.34(5)
P_4Q_4	+2514.04(5)	-1.16(5)
P_2Q_3 (y axis)	0.0	0.0

c) Definition of the x axis

The roll angle of the reference planes on the gun-side flange of the cooling solenoid is -1.86(5) mrad.

d) Additional results

Start of cooling solenoid (gun-side flange surface): y = 754.2(5) mm.

Length of cooling solenoid: 1500.0(5) mm.

"Intersections" with the cooling axis (these are the points on each line which are closest to the y axis):

Line	x	y	z
Gun axis	0.00(1)	415.5(3)	2.0(1)
Collector axis	0.01(1)	2599.8(3)	-1.6(1)

Table 5

Measuring box parameters

Box No.	Position	Number of points			Spacings (mm)			Origin (mm)			Orientation (mrad)			Hall-plate angles (mrad)			
		N_i	N_j	N_k	Δi	Δj	Δk	x	y	z	θ	ϵ	δ	β_1	α_2	β_3	α_3
1	Gun side cooling axis centre	7	79	7	10	20	10	29.8	220.0	30.0	−0.08	0.16	3141.59	−5.20	4.19	−1.59	−1.8
2	Gun side cooling axis displaced	8	40	7	10	20	10	−20.1	220.0	30.3	−0.08	0.16	3141.59	−7.01	6.00	−0.36	−1.6
3	Gun axis centre	7	79	7	10	20	10	−783.6	−716.2	34.2	−627.57	−1.98	3141.71	−5.20	4.19	−1.80	0.0
4	Gun axis displaced	7	31	7	10	20	10	−268.1	96.0	32.6	−627.57	−1.98	3141.71	−7.01	6.00	−0.86	0.8
5	Collector side cooling axis centre	7	79	7	10	20	10	−30.2	2801.4	30.3	3141.80	−0.15	3141.59	−7.02	6.01	−2.35	−6.0
6	Collector side cooling axis displaced	7	40	7	10	20	10	29.8	2801.4	30.3	3141.80	−0.15	3141.59	−9.26	8.25	−0.95	−8.0
7	Collector axis centre	7	60	6	10	20	10	518.2	3365.1	19.1	2514.08	−1.01	3141.47	−7.16	6.15	−2.41	−5.3
8	Collector axis displaced	7	45	6	10	20	10	390.4	3087.1	18.6	2514.08	−1.01	3141.47	−8.26	7.25	−0.58	−6.6
9	Collector axis extension	5	45	5	8	20	8	823.3	3761.6	15.6	2514.02	−0.93	3141.47	−6.72	5.71	−2.27	−
10	Collector side cooling axis extension	7	39	11	9	20	10	−27.0	3331.4	50.0	3141.28	−0.44	3141.59	−6.04	5.03	−2.32	−2.6

Table 6

Fraction of the magnet current passing through
the third coil layers of the toroids and through
the end-effect coils, after adjustment

	Toroid	End-effect coil
Gun side	0.462	0.146
Collector side	0.512	0.118
Nominal	$0.460^{a)}$	–

a) $2R/(R-a-b/2) - 2$. Compare reduction
factor in Table 1.
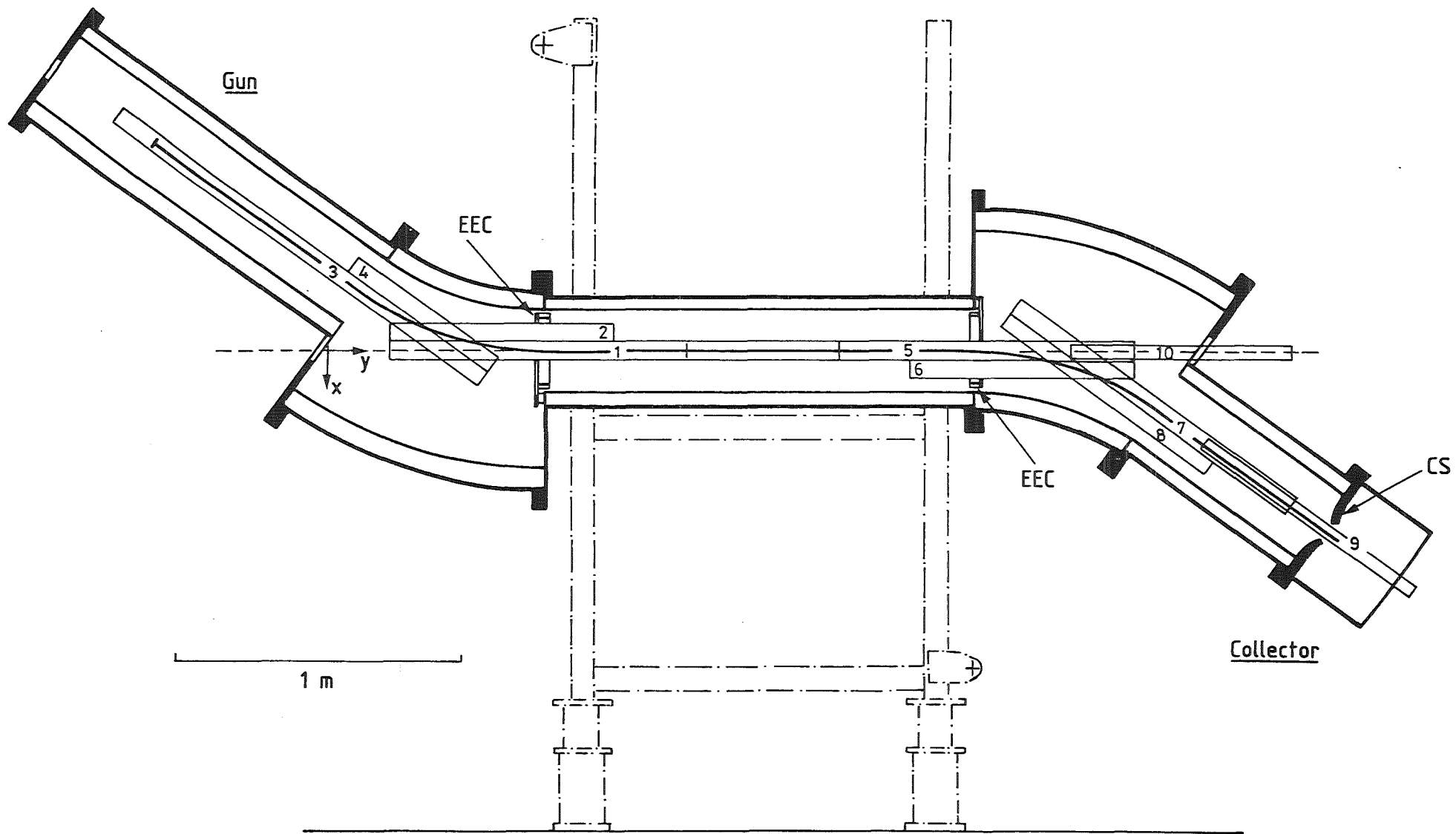
Fig. 1 The magnet assembly, including end-effect coils (EEC), screening plates at gun solenoid and toroids, and the magnetic shunt at the collector (CS). The centre line of the electron beam and the limits of the measuring boxes (1-10) for the field map are also shown.
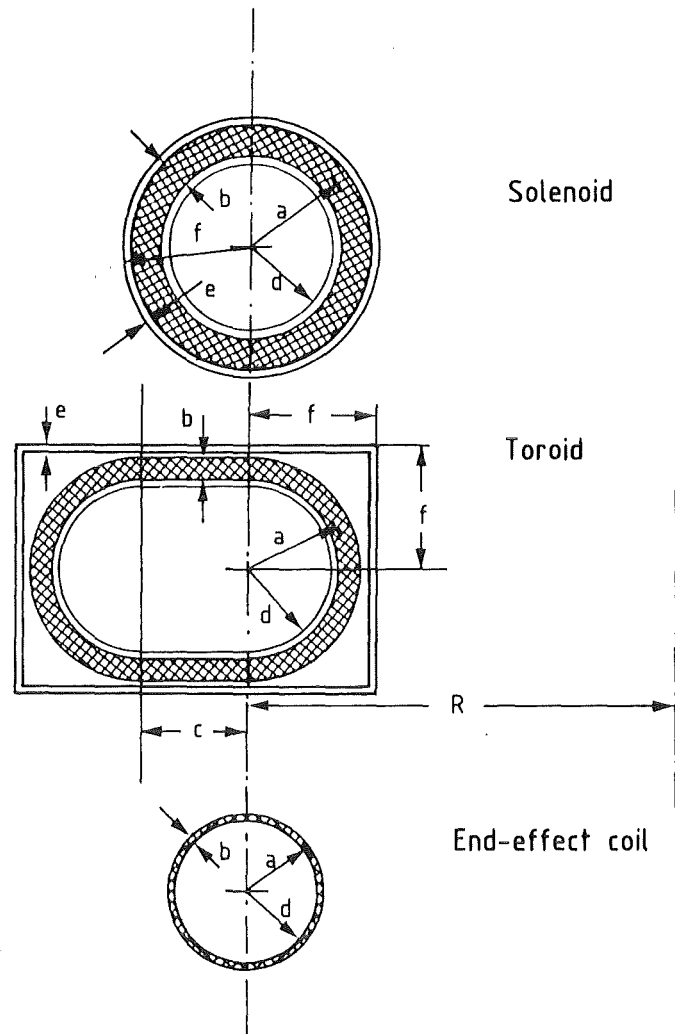
Fig. 2 Cross-sections of magnet coils and screening tubes, the dimensions are given in Table 1.
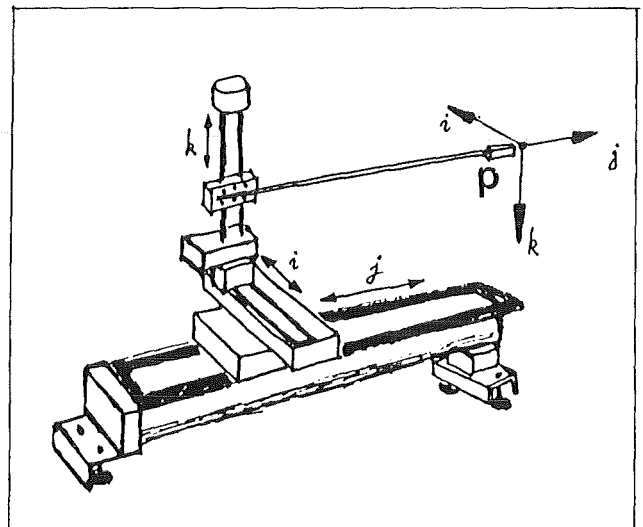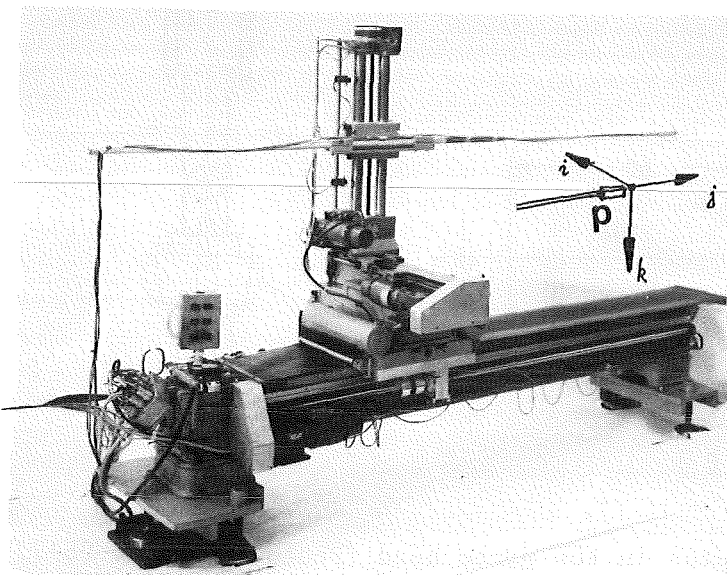
Fig. 3 The scanning apparatus with probe P. The orientation of the reference frame ijk is defined by the sliding rails as shown (Photo CERN 243-5-74).
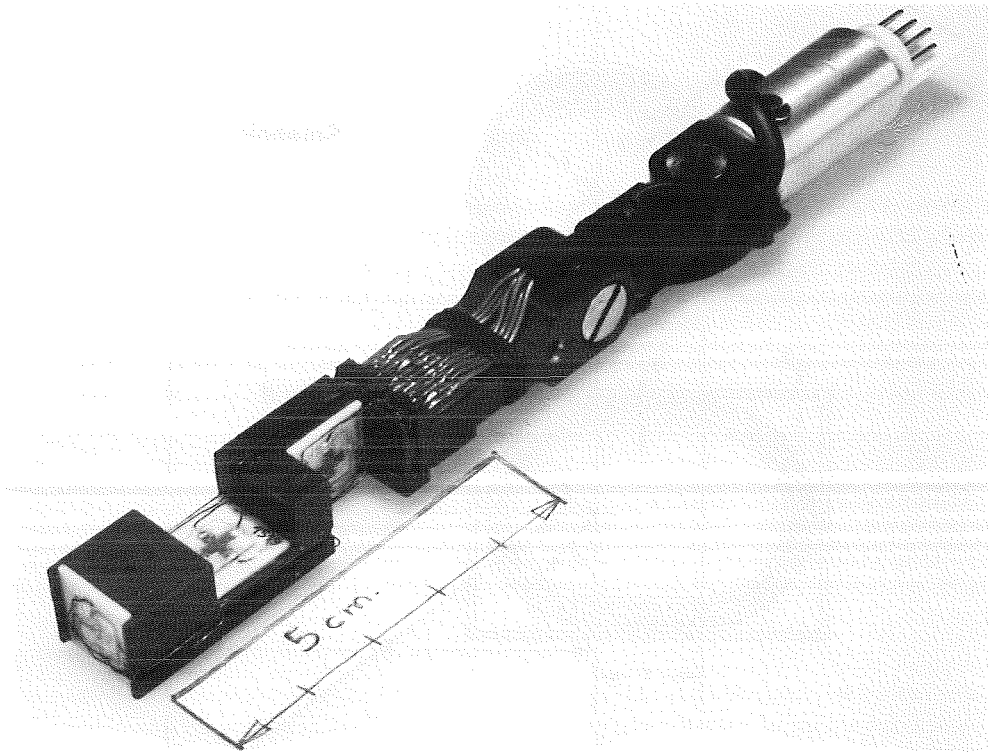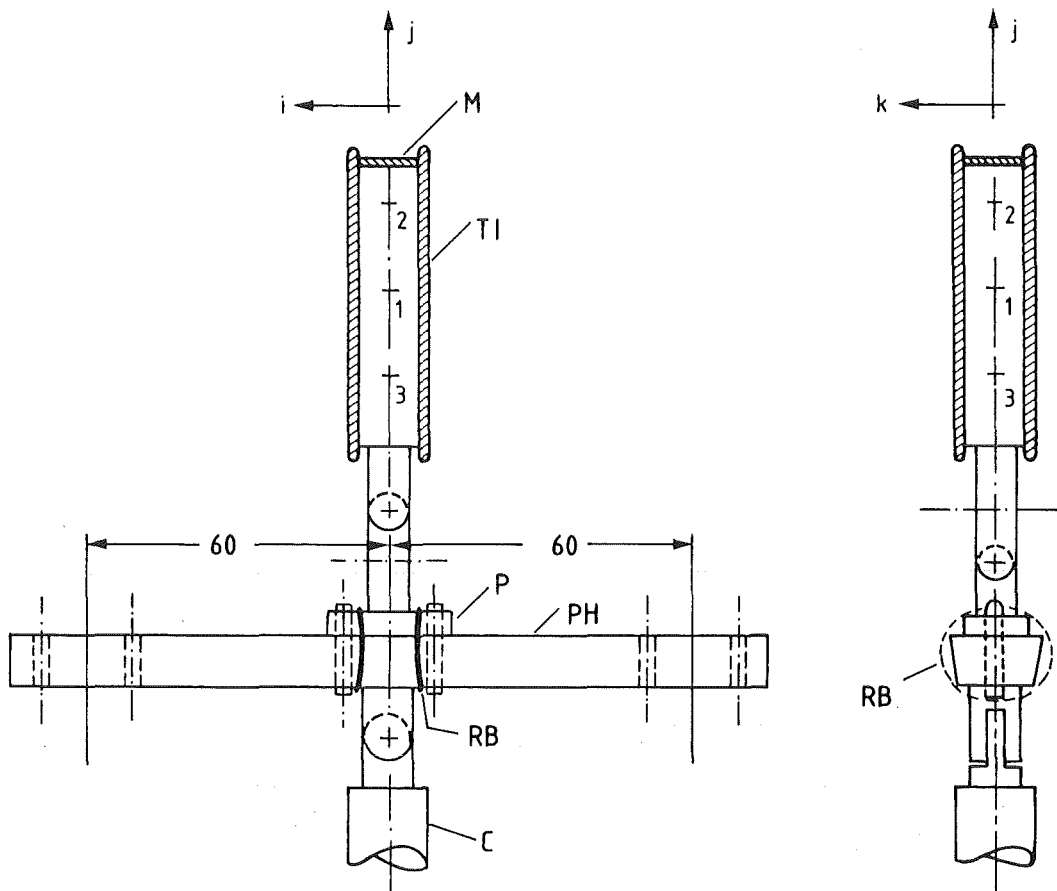
Fig. 4 a) Arrangement of the Hall plates in the probe head (Photo CERN 382-06-77);
b) Probe head assembly with Hall plates 1-3 in a thermal insulation TI, and front
mirror M. The head is mounted on the probe holder PH by a plug P which is pressed
onto the precisely manufactured front plane of PH by a rubber band (RB). The tip
of the ceramic tube C is also shown.
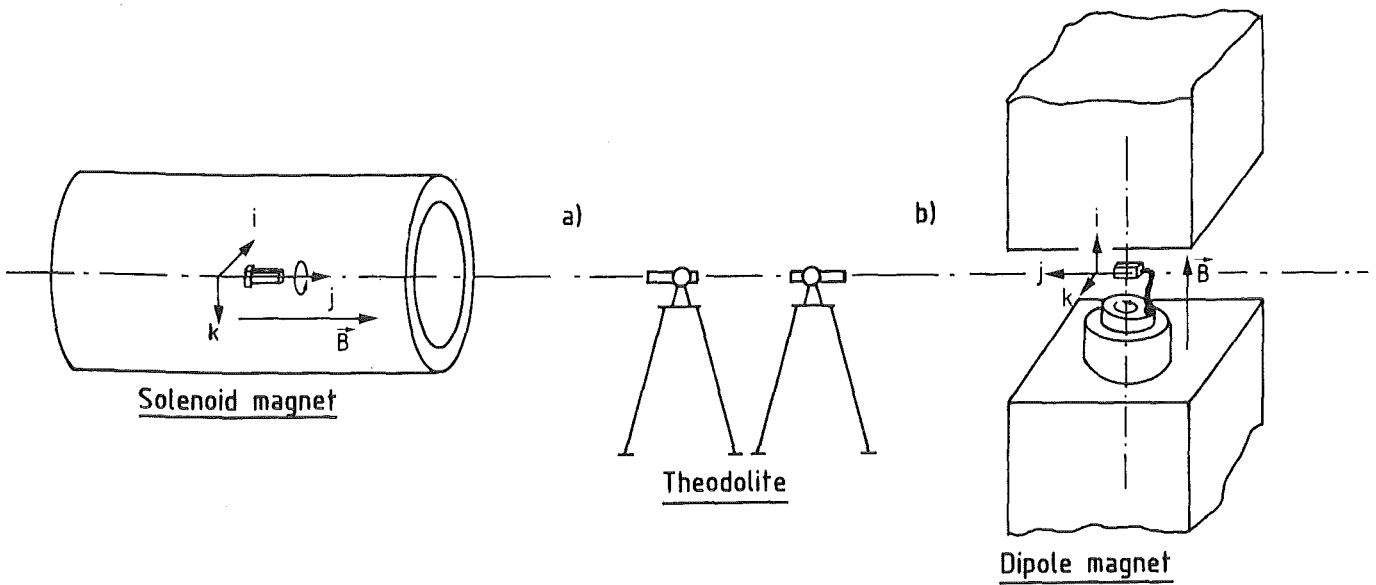
Fig. 5 Set-ups for the determination of Hall-plate misalignments as described in the text, by: a) rotation of the probe about the j axis, b) rotation about the i axis.

Position	Box
A	1,2
B	3,4
C	5,6,10
D	7,8,9
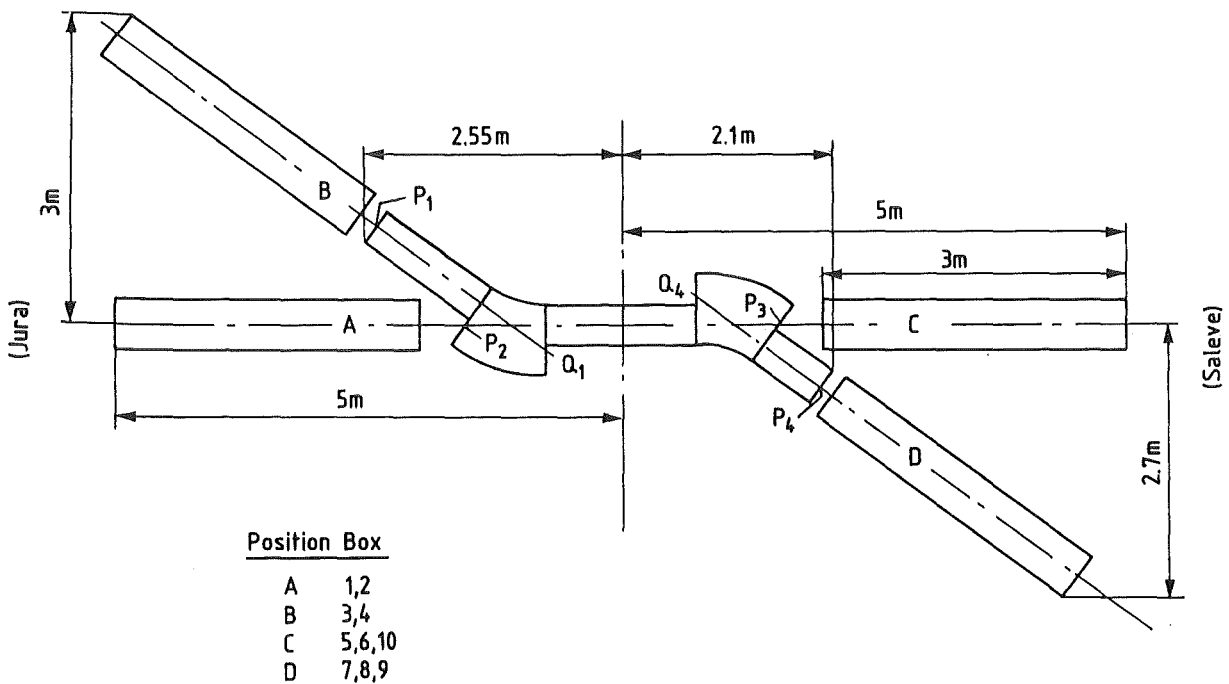
Fig. 6 Ground plan of the measuring site showing magnet reference points P_i, Q_i (see text) and the positions of the scanning device (A-D) for the measurement of the field map boxes.
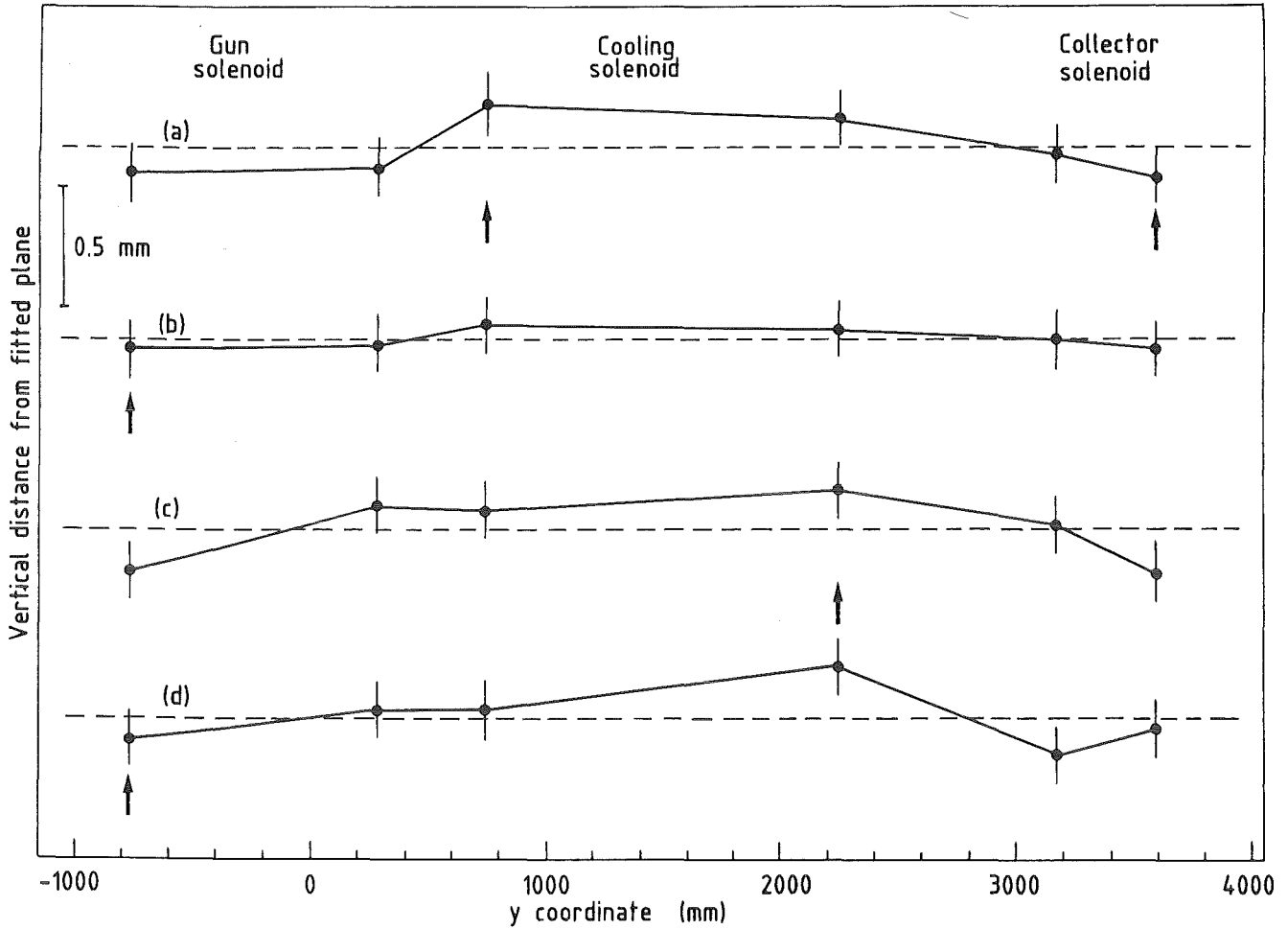
Fig. 7 Vertical deviations of test points on the magnet flanges from a fitted plane (magnet deformation test). The test points and the positions of mechanical supports (arrows) are plotted over their y coordinates for different support arrangements (a-d); d is the final situation.

$$\varphi_1=-d_T/l_T \qquad d_T=\varphi_T \cdot l_0$$

$$\varphi_2=(d_{D'}-d_D)/(l_{D'}-l_D) \qquad d_D=\varphi_D \cdot l_D \qquad d_{D'}=\varphi_{D'} \cdot l_{D'}$$
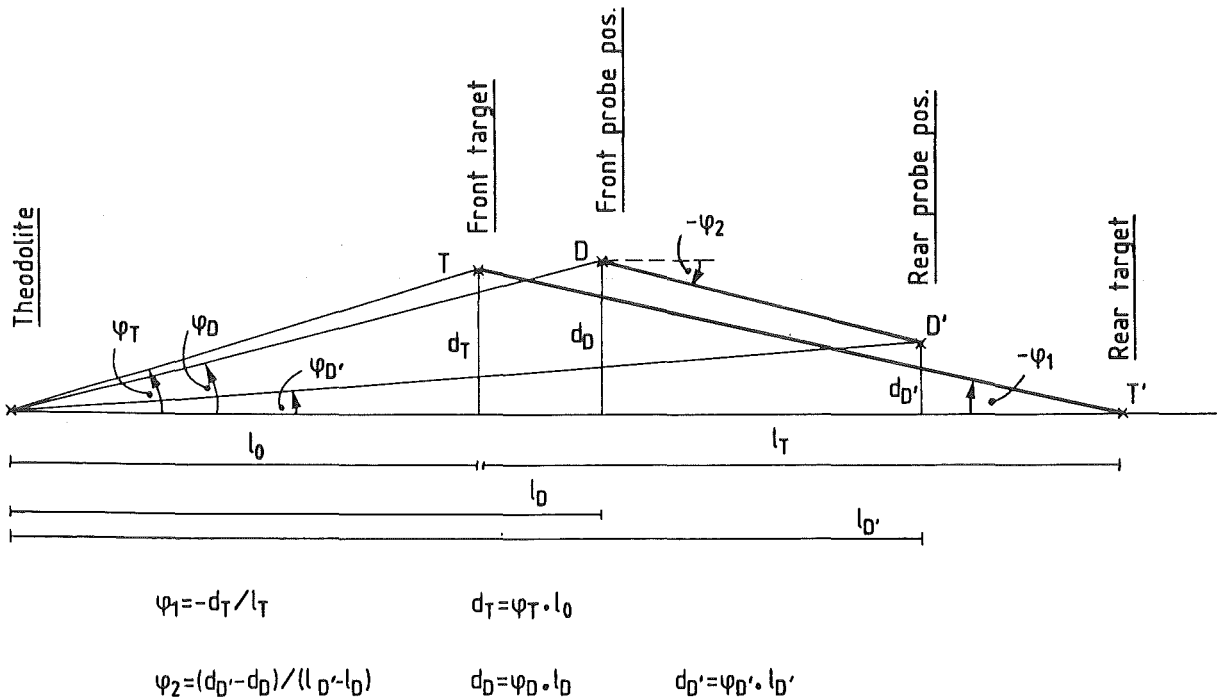
Fig. 8 Determination of the scan axis DD' relative to the known target axis TT' from theodolite readings ϕ_T, ϕ_D, $\phi_{D'}$. The same construction is used for horizontal and vertical angles, which are all assumed to be $\leq$ 10 mrad.

$$B_y = B_0(R/r) \cdot \cos\varphi$$

$$\cos\varphi = R/r$$

$$r^2 = R^2 + (y - y_T)^2$$
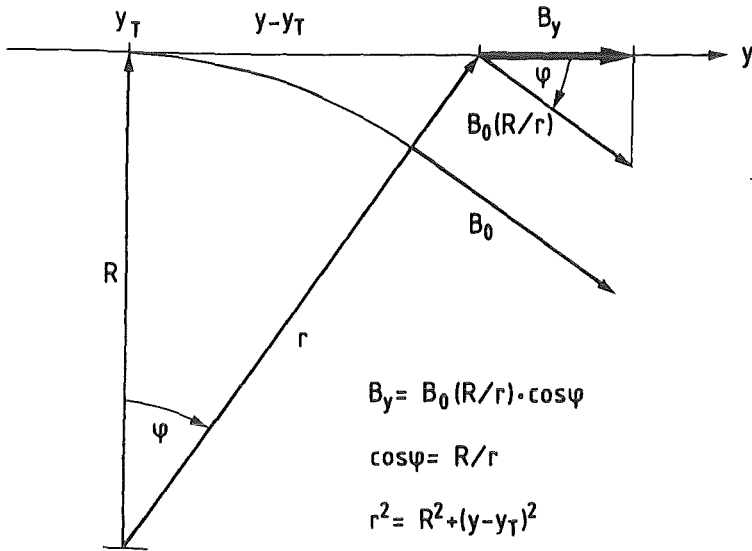
Fig. 9 Calculation of the field strength B_y in the toroids, assuming a perfect toroid field.
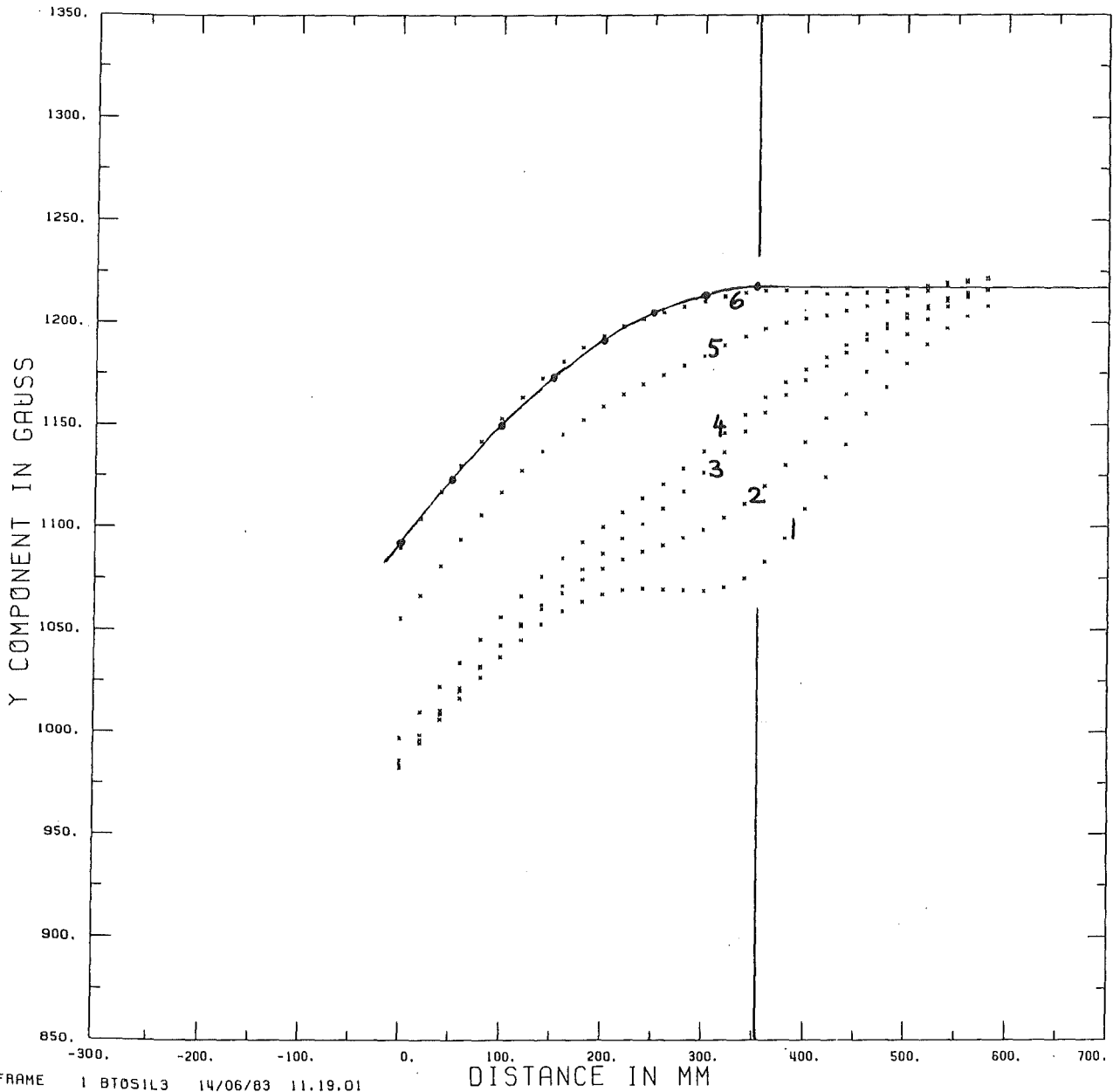
Fig. 10 Field trimming at the gun toroid as described in the text. The vertical line indicates the solenoid/toroid junction.

Fig. 11a Field component B_y in the gun toroid, measured and calculated [line from Eq. (9)].

- 39 -
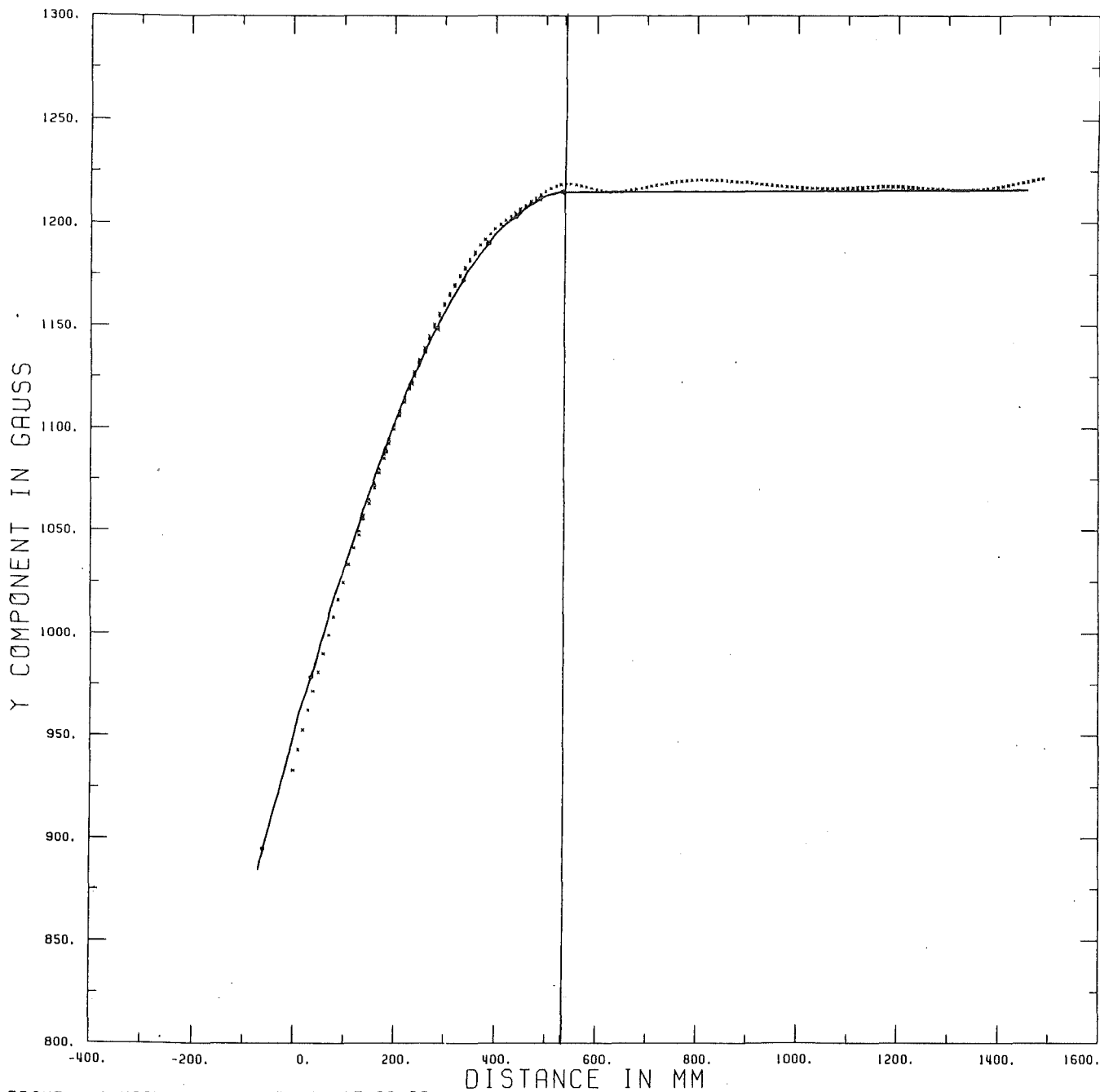
FRAME   6 MAGNE2C   11/07/83 17.09.39   DISTANCE IN MM
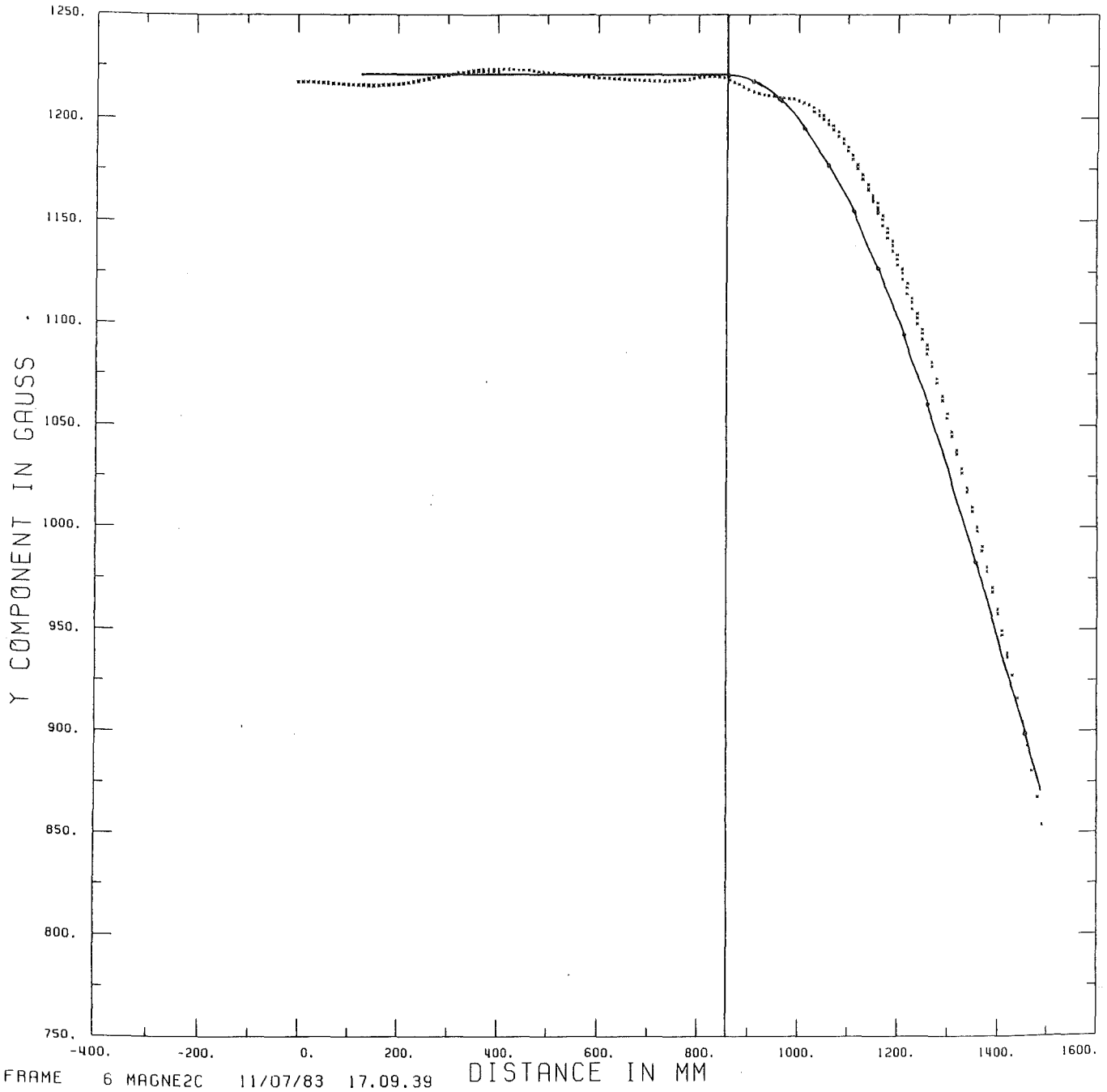
Fig. 11b Field component B_y in the collector toroid, measured and calculated [line from Eq. (9)].
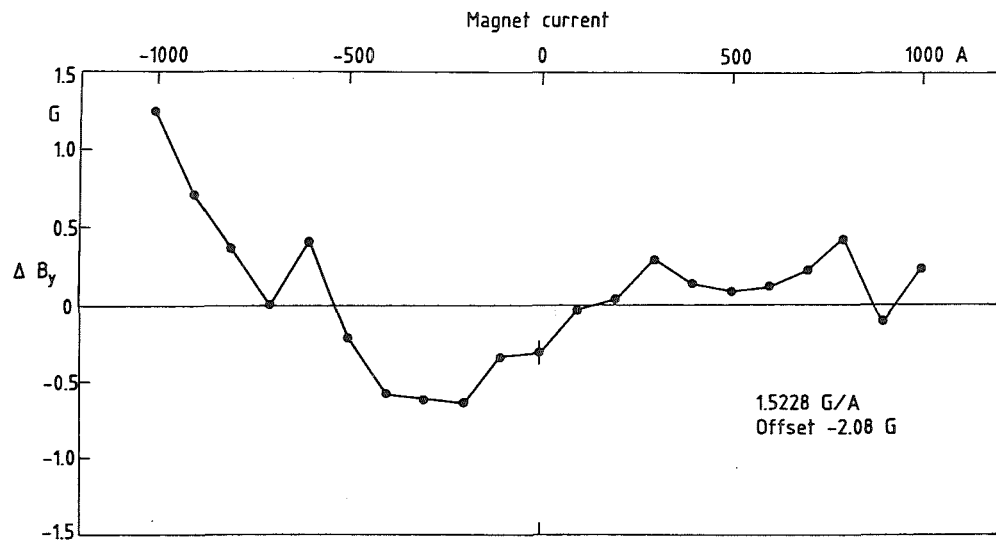
Fig. 12   Longitudinal field strength at the centre of the cooling solenoid measured for varying magnet currents.   The deviations of the measured points from a fitted straight line with the parameters given are plotted.

1.5228 G/A
Offset −2.08 G
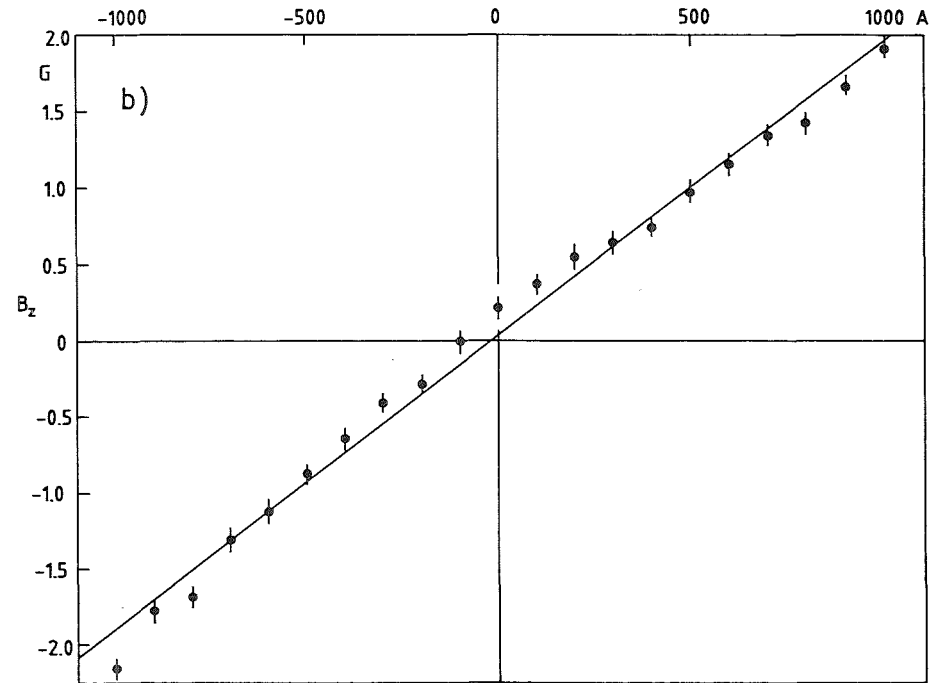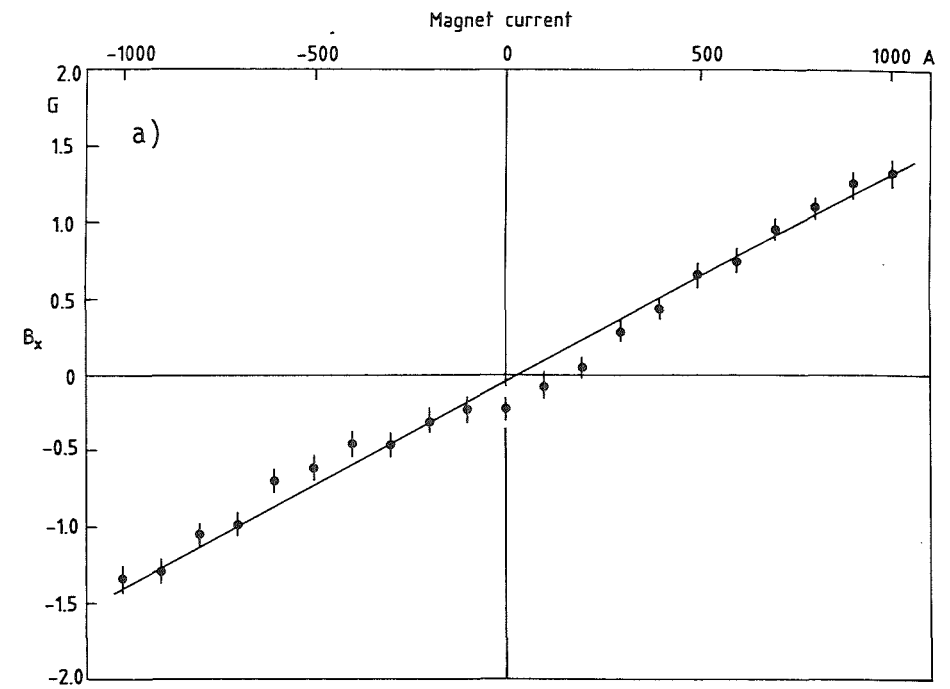
Fig. 13   Transverse field in the cooling solenoid measured for varying magnet currents; a) x component, b) z component.
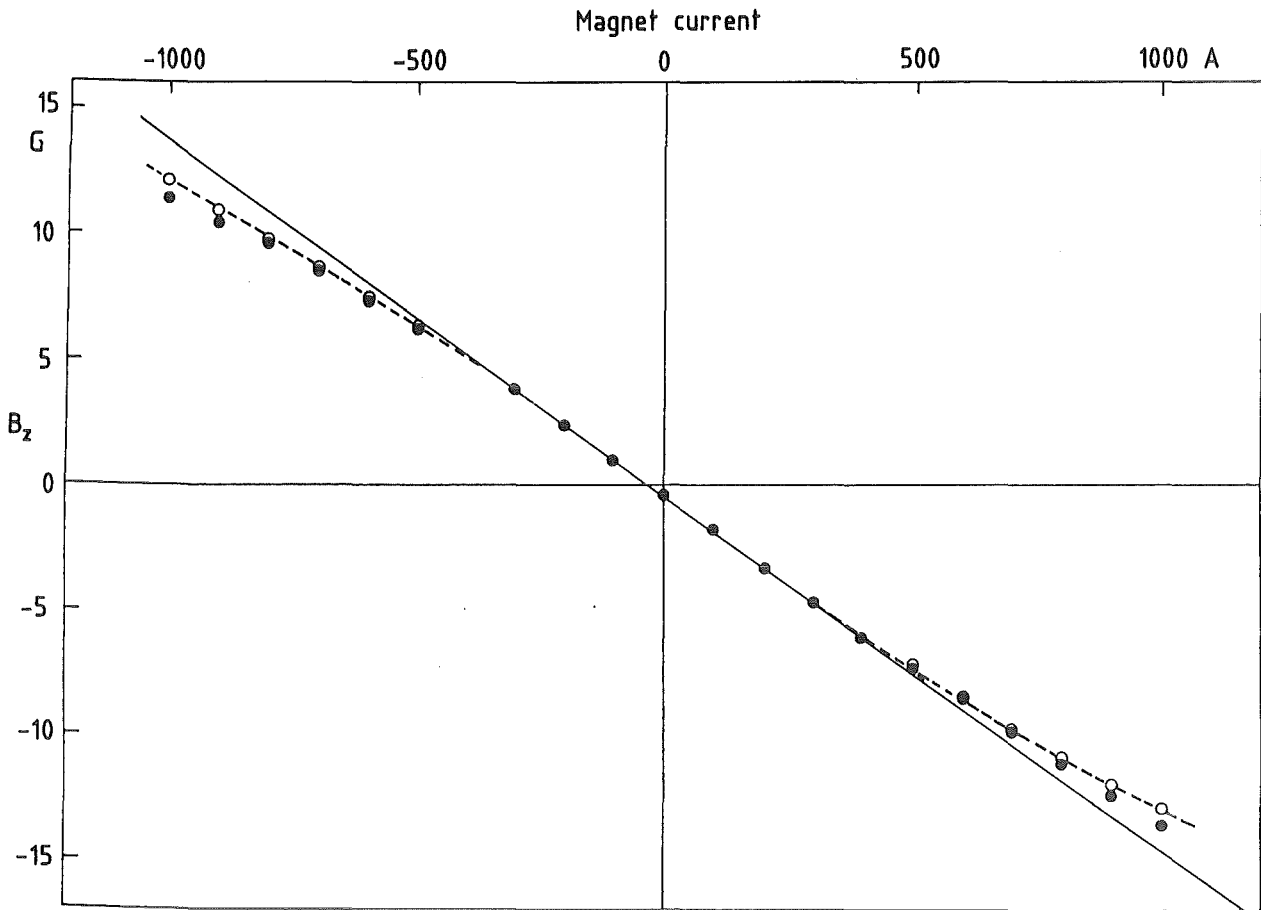
Fig. 14 z component of the magnetic field in the collector toroid measured for varying the magnet current (full circles: measured points, open circles: after subtraction of symmetrical contributions, see text).
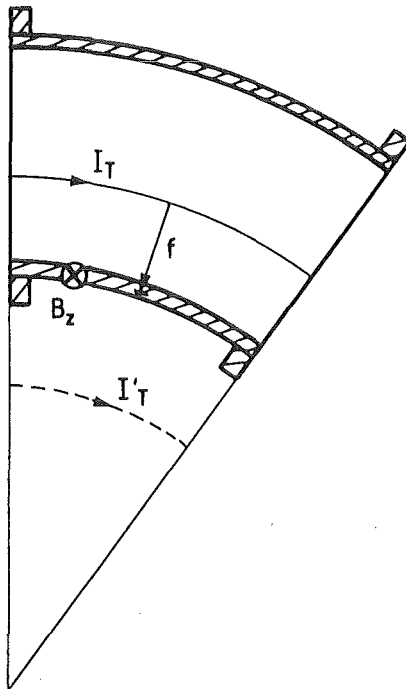
Fig. 15 Estimation of the magnetic field in the z direction produced by the current in the third toroid coil layer (see text).
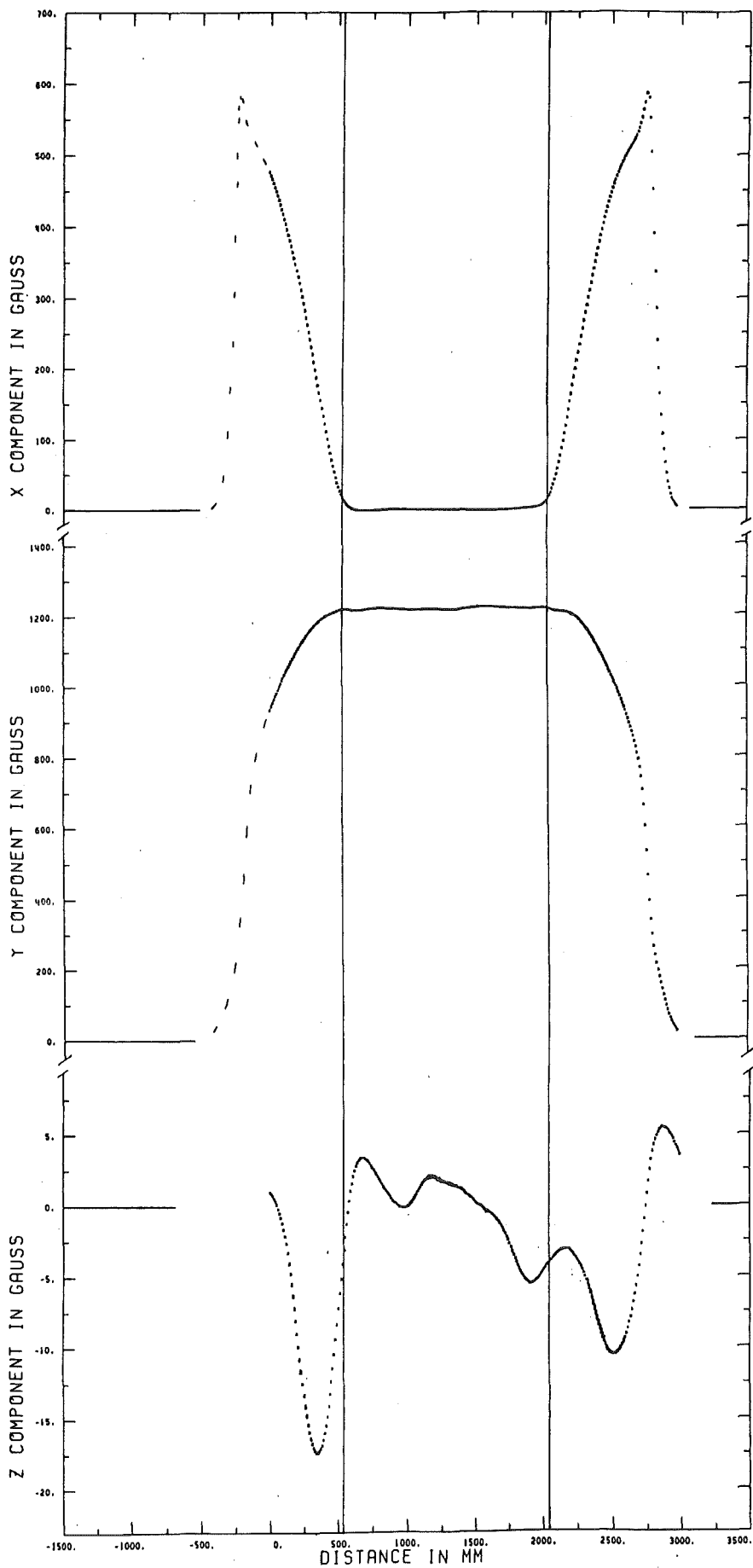
Fig. 16 Magnetic field components measured along the cooling axis (ion trajectory).
The vertical lines indicate the limits of the cooling solenoid.
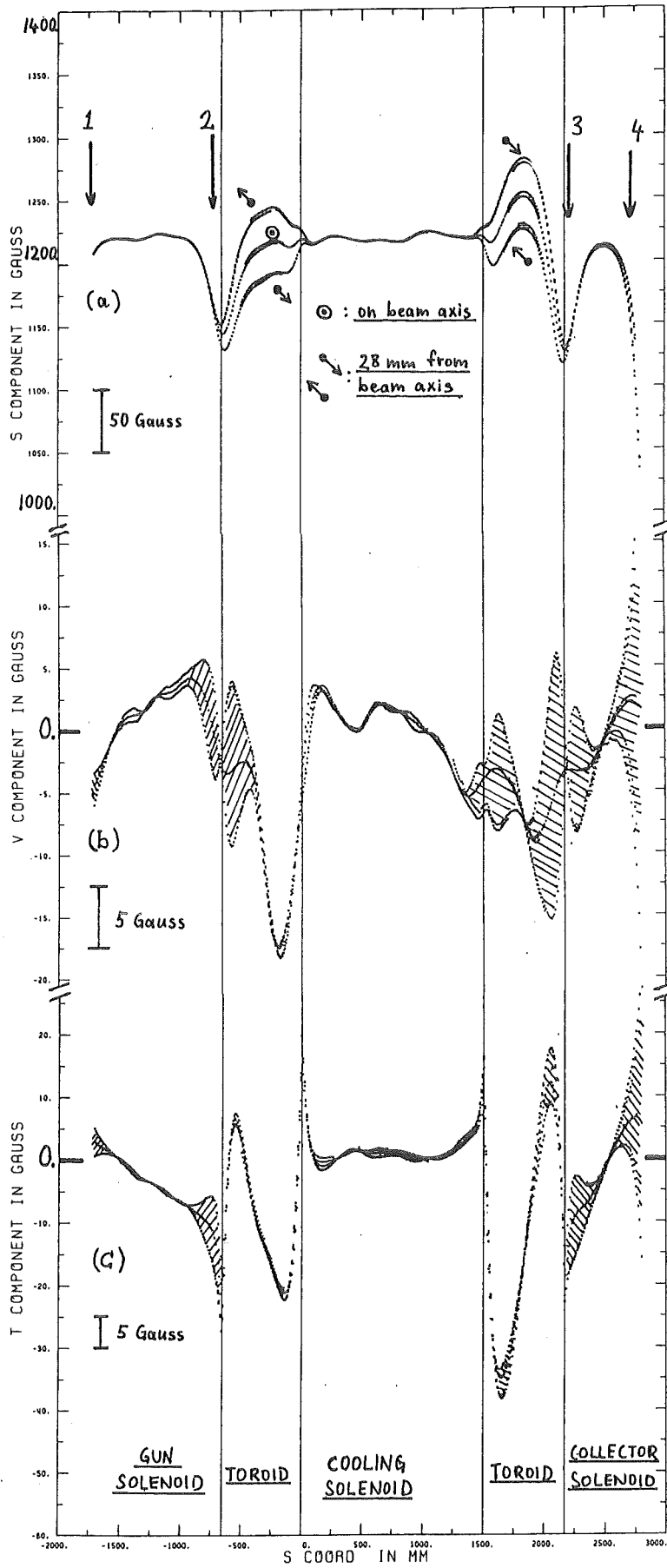
Fig. 17 Magnetic field components along the electron beam:
a) Longitudinal component;
b) Transverse component perpendicular to the bending plane of the toroids;
c) Transverse component in the bending plane of the toroids.
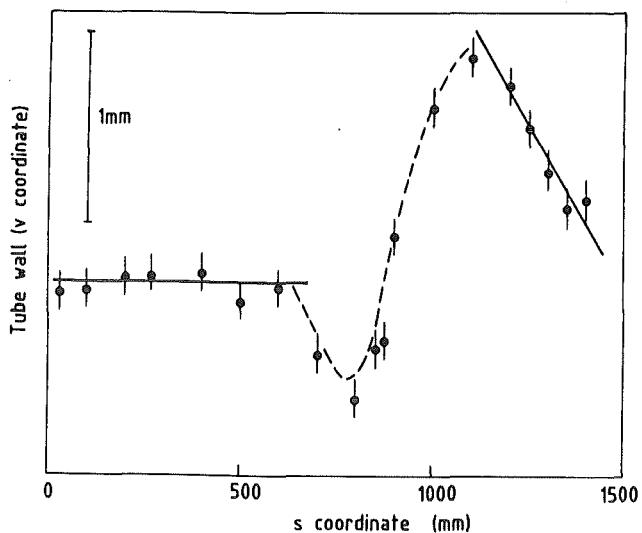
Fig. 18 Profile of the outer wall of
the cooling solenoid screening tube
measured along a straight line with
s ≈ 0, v ≈ 200 mm.
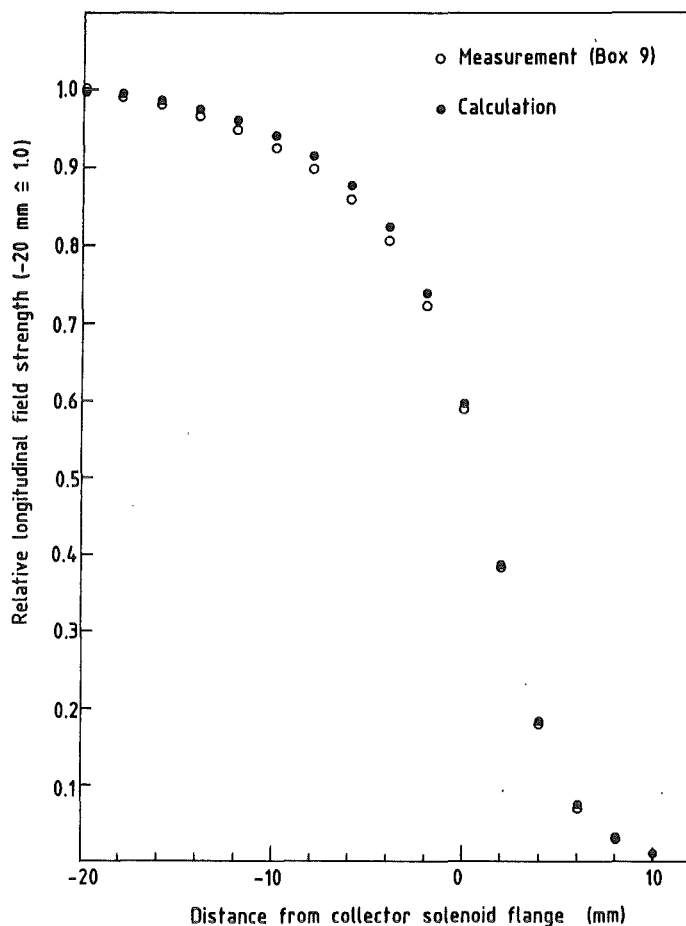
Fig. 19 Measured and calculated lon-
gitudinal field strength at the collec-
tor entrance (normalized results).
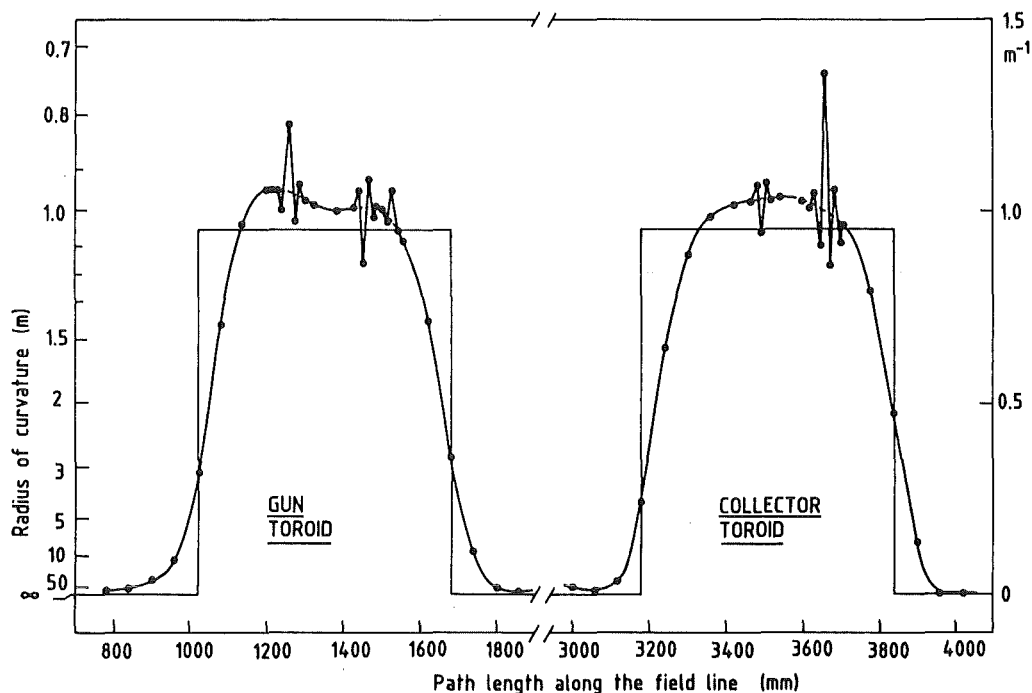
Fig. 20 Radius of curvature of a field line started in the gun solenoid along its
path through the toroids.
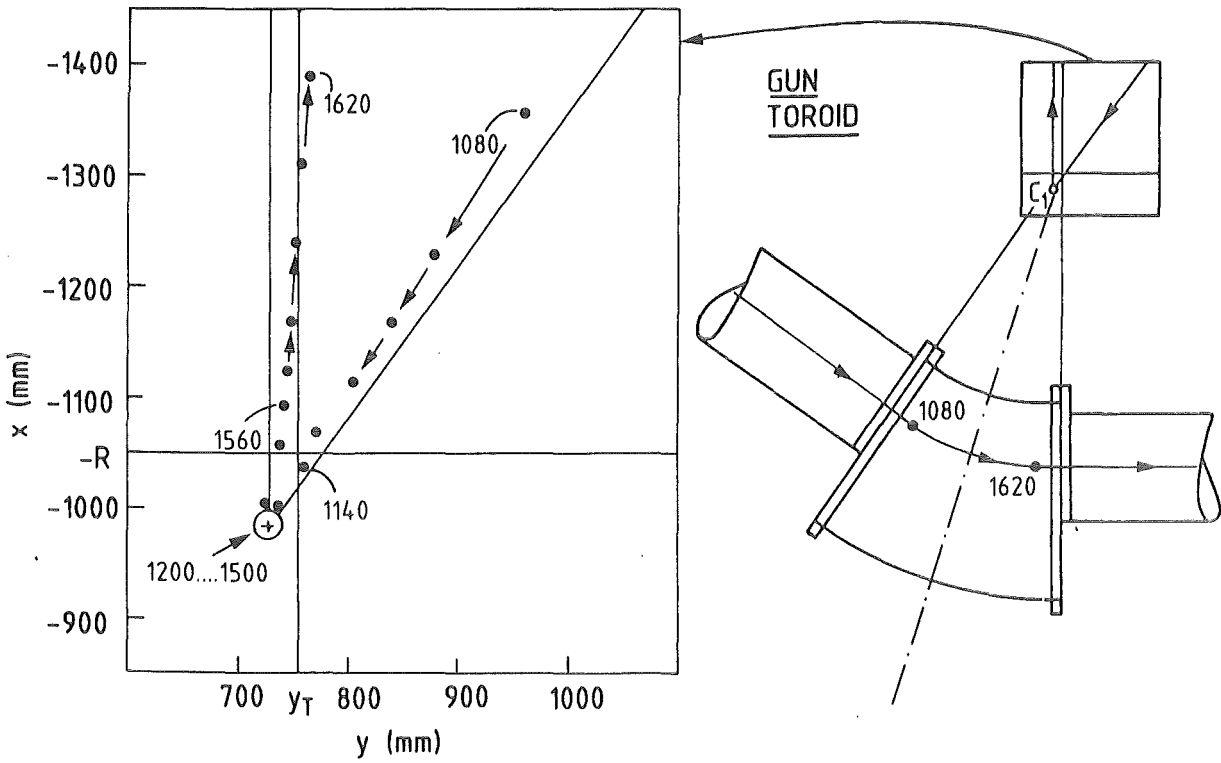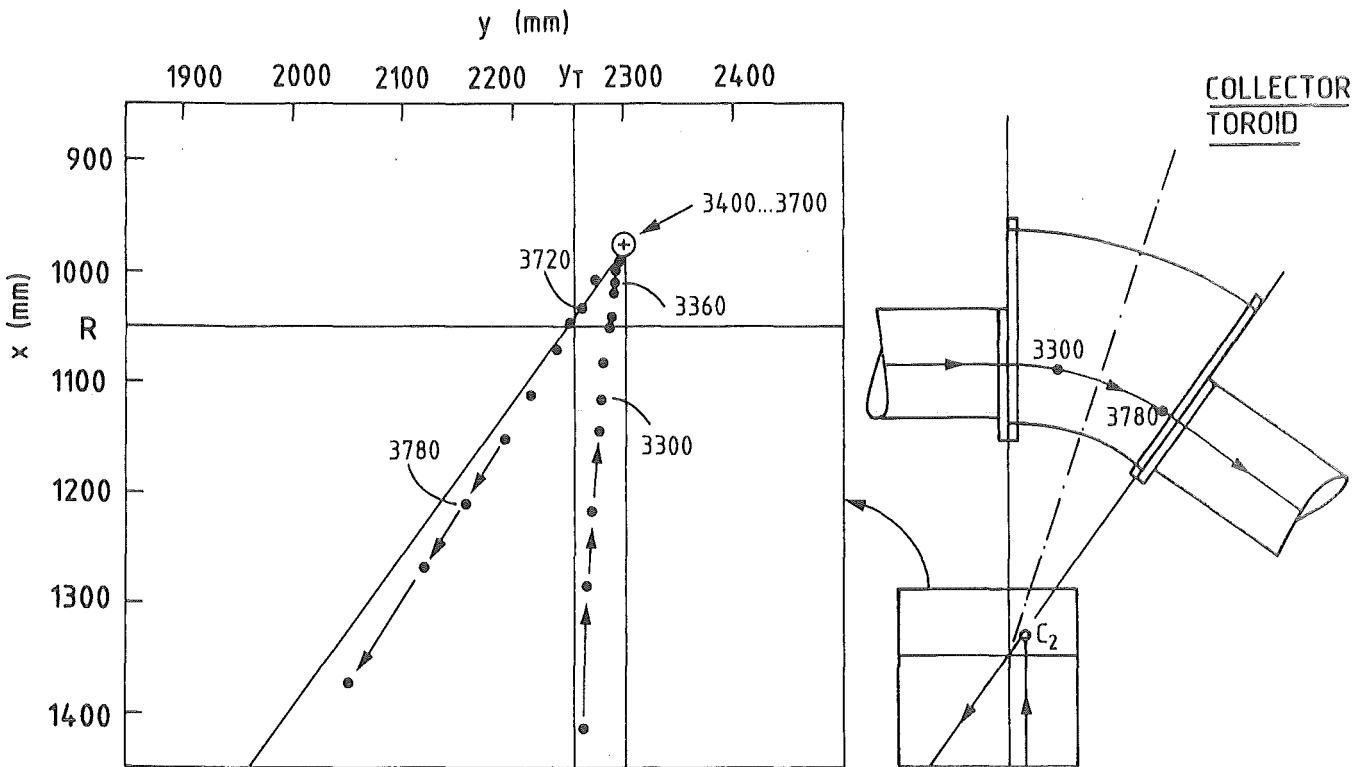
Fig. 21 Map showing instantaneous positions of the centre of curvature in the toroid bending plane along the path of a field line. Arrows show the sense in which the field line is followed, and numbers indicate the path length along the line in mm. a) Gun toroid, b) collector toroid.

Fig. 22 Field lines started in a plane corresponding to the cathode of the electron
gun. a) Lines started with horizontal displacements from the cathode centre, and
shown in horizontal projection and in special coordinates (Appendix 3). b) Lines
started with vertical displacements and shown in vertical projection. The field
line from the cathode centre is marked by arrows. The bending plane of the toroids
is in the horizontal plane (measuring position).

ANGLE CONVENTION FOR SURVEY AND SCANNER COORDINATES

The scanner coordinate frame ijk is obtained by three rotations of the general xyz frame. The first two rotations fix the longitudinal scan direction (j-axis); they are performed about the z axis by an angle θ (often large), and about an intermediate x' axis (perpendicular to i and j after the first rotation), by an angle ε which will always be small since all magnet axes approximately lie in the xy plane. The third rotation, about the longitudinal scan direction j, defines the transverse scan axes. Such a sequence of rotations differs from the Euler angle convention in which the longitudinal scan direction would be less clearly defined. It rather corresponds to a so-called 'xyz convention' often used to describe the orientation of a vehicle[10].

The matrix M for the transformation to the ijk frame of vector components given in the xyz frame is obtained as a product of three elementary rotation matrices $R_u(\alpha)$ (counter-clockwise rotation by α about axis u):

$$M = R_j(\delta)R_{x'}(\varepsilon)R_z(\theta) =$$

$$= \begin{pmatrix} \cos\theta\cos\delta - \sin\theta\sin\varepsilon\sin\delta & \sin\theta\cos\delta + \cos\theta\sin\varepsilon\sin\delta & -\cos\varepsilon\sin\delta \\ -\sin\theta\cos\varepsilon & \cos\theta\cos\varepsilon & \sin\varepsilon \\ \cos\theta\sin\delta + \sin\theta\sin\varepsilon\cos\delta & \sin\theta\sin\delta - \cos\theta\sin\varepsilon\cos\delta & \cos\varepsilon\cos\delta \end{pmatrix}$$

The rows of M are the coordinates of the scanner axes i,j,k in the xyz frame. The angles θ, ε, and δ are named azimuth, pitch, and roll, respectively. By definition, all rotations are right-handed about their axes. The angle ε ranges from $-\pi/2$ to $\pi/2$ only, and for positive ε the j axis is rising from the xy plane.

The angles θ and ε are also used to give the direction of axes determined by survey.

APPENDIX 2

COMPUTER EVALUATION OF THE MAGNETIC MEASUREMENTS

The data evaluation is schematically shown in Fig. A.1. The upper part of the diagram represents the slightly modified standard evaluation of the CERN Magnetic Measurement Control System[5], running on the IBM system. The program MMEAS has been changed to allow a resolution smaller than 1 G for the magnetic field values. MMREC is a version of MMEAS which allows one to access single line scans ("records") rather than complete volume scans ("runs"). The magnetic field values (in gauss) are written to disk files in coded (card image) format.

The evaluation then proceeds with the programs described in the following. Subroutines used by these programs for some standard tasks are available in a library MAGLIB. At present, the evaluation programs are installed at the CDC computer system at CERN.

i) *Programs handling uncorrected data*

Uncorrected data files in coded form are read by subroutine READMM in MAGLIB which writes the field components into an array. If requested, READMM averages results with positive and negative magnet current [Eq. (1)].

MMBOX

applies the correction according to Eq. (3) to uncorrected averaged data. Hall-plate angles are expected as input. The results of one scan volume are stored on a random mass storage output file (field map) by adding or replacing one record. For the complete information on one such *data box*, also the orientation and origin coordinates of the scanner frame, as found by survey, are expected as input and written to the output file. Records are added or replaced by subroutine STORE (MAGLIB).

OVRLAP

compares uncorrected data in two overlapping boxes, the relative position of which must be input. It allows the determination of α_3 from Eq. (7). α_3 is needed as input for MMBOX.

PRBOX

interpolates, lists and plots uncorrected data. The results presented in Section 3.1 and 3.2 are obtained this way.

ii) Programs handling the field map (corrected data)

The random mass storage file containing the field map is filled and updated by MMBOX (see above), and initialized by running the program CREATE (in MAGLIB).

FPLOT

interpolates, lists and plots data of the mass storage field map. Field components B_x, B_y, B_z and "field angles" B_x/B_y, B_z/B_y are displayed. The program runs in cycles for each of which the following specifications can be given:

- Display data along a straight line given by direction and starting point.

- Show data from all or from selected boxes.

- Calculate field components in a given constant reference frame.

- Display data along a trajectory corresponding to the electron cooling geometry (Appendix 3).

- Calculate the field components in a frame accompanying the trajectory.

- Plot field data together with the data of the next cycle(s).

- Calculate integrals of the field components over a straight line or trajectory, between specified limits.

TRACK

follows a field line, as described in Section 3.5, through the volume covered by the mass storage field map. A field line is started by giving input data on the starting point coordinates, the distance of the points at which the field line coordinates are calculated ("step"), and the maximum length.

The track algorithm (subroutine FOLLOW) uses the Runge-Kutta routine CERNLIB D203 (INTSTP) to find the second point of the field line, and proceeds with

$$\text{predictor:} \quad \vec{y}_{n+1}^{(P)} = \vec{y}_{n-1} + 2h \cdot \vec{B}_n / B$$

$$\text{corrector:} \quad \vec{y}_{n+1}^{(C)} = \vec{y}_n + (h/2)(\vec{B}_{n+1}/B + \vec{B}_n/B)$$

where

$$\vec{B}_{n+1} = \vec{B}\left(\vec{y}_{n+1}^{(P)}\right), \quad \vec{B}_n = \vec{B}(y_n), \text{ and n is the point index.}$$

The new field line point is taken as

$$\vec{y}_{n+1} = 0.8\ \vec{y}_{n+1}^{(C)} + 0.2\ \vec{y}_{n+1}^{(P)}$$

and the error estimate as:

$$\varepsilon_{n+1} = \left|\vec{y}_{n+1}^{(P)} - \vec{y}_{n+1}^{(C)}\right| .$$

This method[11] eliminates errors of second order in the step length h.

The points of the field line are written to a sequential file which can hold several field lines started successively. Separate programs plot and list the field lines (PLOTIT, LISTIT).

LISTIT also evaluates the differential geometry of the field line by giving the directions of the tangent and normal vectors; the normal vector is pointing to the instantaneous centre of curvature. This requires the first and second derivatives of the coordinates along the line with respect to the path length, which are found by fitting a third-order spline to the x, y, and z coordinates (subroutine SPLIN3, CERNLIB E209). The radius of curvature and the coordinates of the centre of curvature, which can easily be obtained from the derivatives, are also listed.

COORDINATE TRANSFORMATIONS FOR THE ELECTRON BEAM REFERENCE FRAME

The coordinate transformation depends on seven parameters to be preset which are (see Fig. A.2):

$$
\begin{array}{ll}
\text{origin coordinates} & x_A, \ y_A \\
\text{toroid radii} & R_1, \ R_2 \\
\text{toroid angles} & \phi_1, \ \phi_2 \\
\text{cooling solenoid length} & L
\end{array}
$$

i) *Coordinates of auxiliary points:*

B: $x_B = x_A - R_1(1 - \cos \phi_1)$, $y_B = y_A - R_1 \sin \phi_1$

C: $x_C = x_A$, $y_C = y_A + L_2$

D: $x_D = x_A + R_2(1 - \cos \phi_2)$, $y_D = y_A + L_2 + R_1 \sin \phi_2$

ii) *Transformation* $xyz \to tsv$

a) $y < y_A$: $\phi = \min[\arctan(y_A - y)/(R_1 - x_A + x), \phi_1]$

$\alpha)$ $\phi = \phi_1$: $t = (x - x_B) \cos \phi_1 - (y - y_B) \sin \phi_1$

$s = (x - x_B) \sin \phi_1 + (y - y_B) \cos \phi_1 - R_1 \phi_1$

$\beta)$ $\phi < \phi_1$: $t = \sqrt{(y_A - y)^2 + (R_1 - x_A + x)^2} - R_1$

$s = -R_1 \phi$

b) $y_A \leq y \leq y_C$: $t = x - x_A$

$s = y - y_A$; $\phi = 0$

c) $y > y_C$: $\phi = \min[\arctan(y - y_C)/(R_2 - x + x_C), \phi_2]$

$\alpha)$ $\phi < \phi_2$: $t = -\sqrt{(y - y_C)^2 + (R_2 - x + x_C)^2} + R_2$

$s = L + R_2 \phi$

$\beta)$ $\phi = \phi_2$: $t = (x - x_D) \cos \phi_2 - (y - y_D) \sin \phi_2$

$s = (x - x_D) \sin \phi_2 + (y - y_D) \cos \phi_2 + L + R_2 \phi_2$

For the magnetic field components

$$\begin{pmatrix} B_t \\ B_s \end{pmatrix} = \begin{pmatrix} \cos \phi & -\sin \phi \\ \sin \phi & \cos \phi \end{pmatrix} \begin{pmatrix} B_x \\ B_y \end{pmatrix} ;$$

ϕ depending on y as above.

iii) *Transformation tsv $\rightarrow$ xyz*

a) $s < -R_1\phi_1$:
$\phi = \phi_1$

$x = x_B + t \cos \phi_1 + (s + R_1\phi_1) \sin \phi_1$

$y = y_B - t \sin \phi_1 + (s + R_1\phi_1) \cos \phi_1$

b) $-R_1\phi_1 \leq s < 0$:
$\phi = s/R_1$

$x = x_A - R_1 + (t + R_1) \cos \phi$

$y = y_A + (t + R_1) \sin \phi$

c) $0 \leq s \leq L$:
$\phi = 0$

$x = x_A + t$

$y = y_A + s$

d) $L < s \leq L + R_2\phi_2$:
$\phi = (s - L)/R_2$

$x = x_C + R_2 + (t - R_2) \cos \phi$

$y = y_C - (t - R_2) \sin \phi$

e) $s > L + R_2\phi_2$:
$\phi = \phi_2$

$x = x_D + t \cos \phi_2 + (s - L - R_2\phi_2) \sin \phi_2$

$y = y_D - t \sin \phi_2 + (s - L - R_2\phi_2) \cos \phi_2 .$

For the magnetic field components:

$$\begin{pmatrix} B_x \\ B_y \end{pmatrix} = \begin{pmatrix} \cos \phi & \sin \phi \\ -\sin \phi & \cos \phi \end{pmatrix} \begin{pmatrix} B_t \\ B_s \end{pmatrix} ;$$

ϕ depending on s as above.

iv) Values of the parameters

The nominal values for toroid radii and angles are 1050 mm and 36° (Table 1).

From the survey results (Table 4) we have y_A = 754.2 mm, x_A = 0. More realistic

values for the toroid parameters can be obtained if the measured azimuth angles of

the gun and collector axes are used. Moreover, the radii of the arcs linking the

straight lines can be found from the coordinates of the intersection points of these

axes with the cooling axis; these values are also given in Table 4, and $R = d/\tan(\phi/2)$

(see Fig. A.2). The parameters determined in this way are

$$R_1 = 1043.4 \text{ mm}, \quad \phi_1 = 35.968°,$$

$$R_2 = 1065.0 \text{ mm}, \quad \phi_2 = 35.956°.$$

They have been used for presenting the results in Sections 3.3.3 and 3.5.
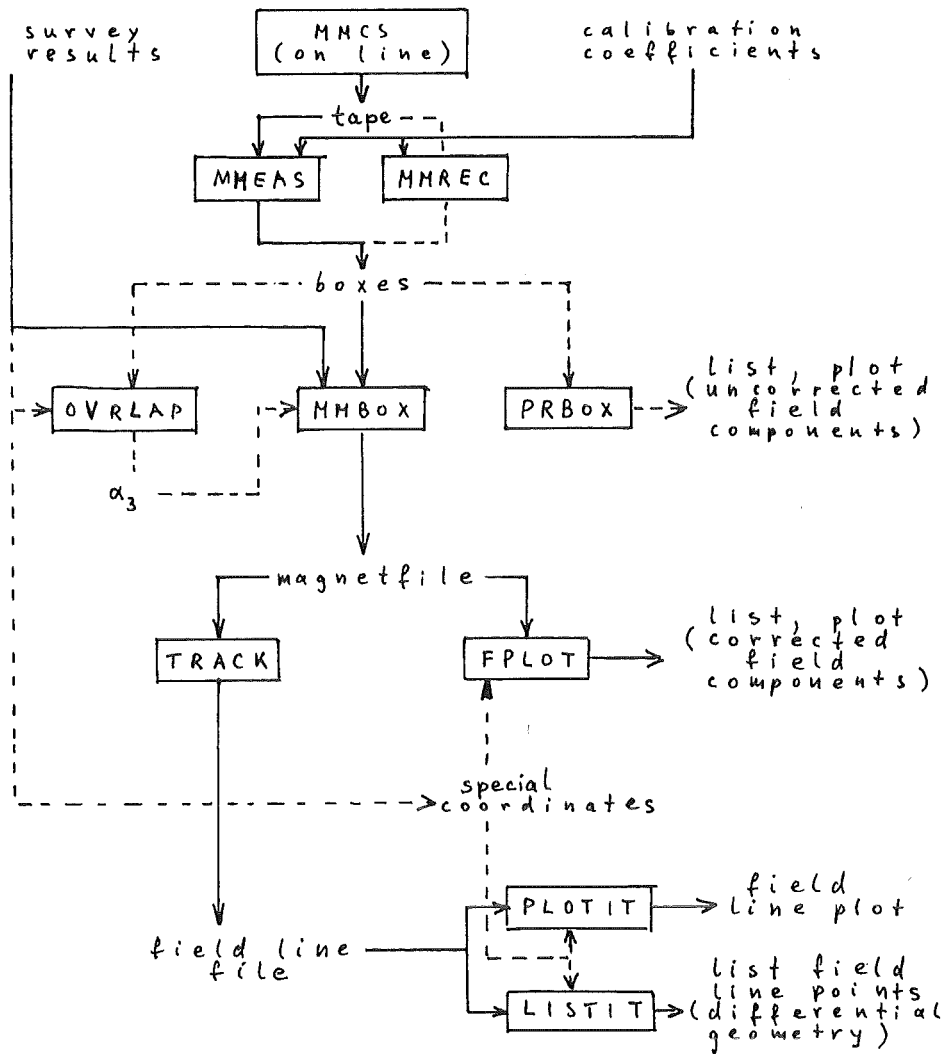
Fig. A.1 Data flow chart showing programs and data sets used for the evaluation.
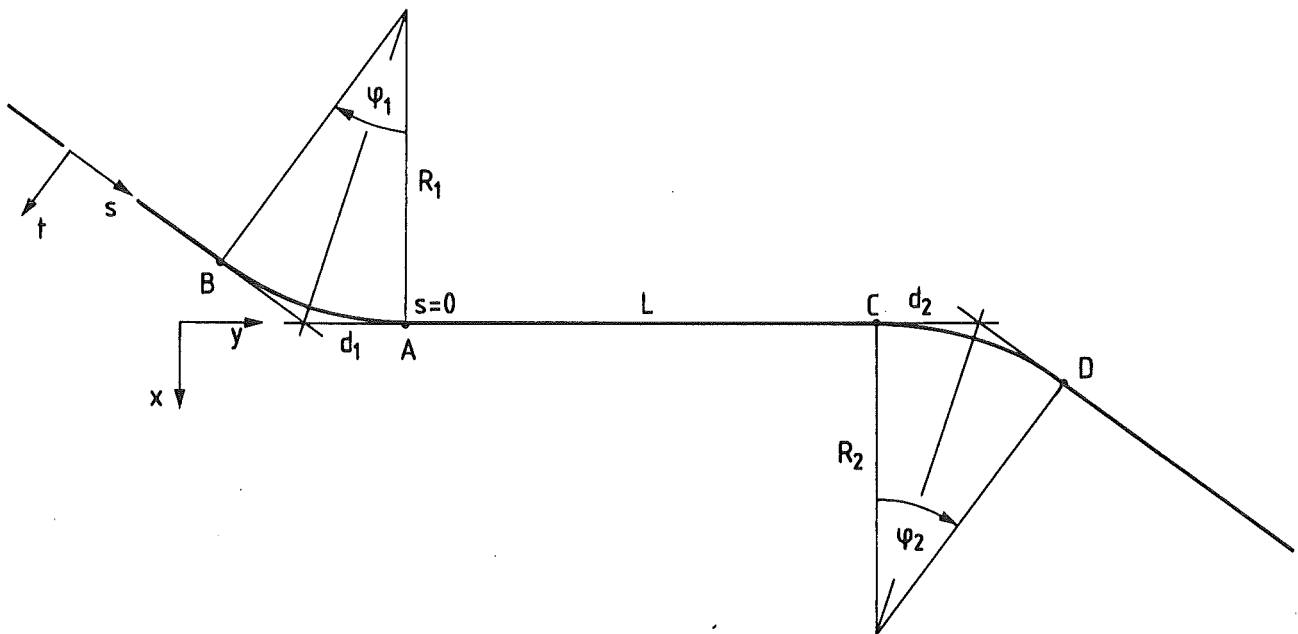
Fig. A.2 Reference points and parameters of the special coordinates for the electron cooling geometry.

REFERENCES

1) L. Hütten, H. Poth, A. Wolf, H. Haseroth and Ch. Hill, The electron cooling
   device for LEAR, *in* Proc. Workshop on Physics at LEAR with Low-Energy
   Cooled Antiprotons, Erice, 1982 (ed. U. Gastaldi), in press.

   L. Hütten, H. Poth, A. Wolf, H. Haseroth, Ch. Hill and J.L. Vallet, The status
   of the electron cooling device for LEAR, *in* Proc. 12th Int. Conf. on High-
   Energy Accelerators, Batavia, Ill., 1983, to be published.

2) M. Bell, J. Chaney, H. Herr, F. Krienen, P. Møller-Petersen and G. Petrucci,
   Nucl. Instrum. Methods <u>190</u>, 237 (1980).

3) Ya.S. Derbenev and A.N. Skrinskii, Part. Accel. <u>8</u>, 235 (1978).

4) O. Runolfsson, Magnet measurements in high-energy experiments, *in* Proc. Sixth
   Int. Conf. on Magnet Technology, Bratislava, 1977 (ALFA, Bratislava, 1978),
   p. 802.

5) J. Schinzel, MMCS users guide, CERN/DD/OC/GA 80-4 (1981).

6) D. Grijo dos Santos, Fitting Hall probe measurements, CERN/EP/DHR 77-4 (1977).

7) Yu.L. Kiselev, N.A. Burgov, S.A. Gerzon, Yu.V. Terekhov, V.I. Ushakov and
   M.M. Chumakov, Nucl. Instrum. Methods <u>119</u>, 323 (1974).

8) K.J. Hume, Metrology with autocollimators (Hilger and Watts, London, 1965).

9) C. Iselin, Solution of Poisson's or Laplace's equations in two-dimensional
   regions, CERN Computer Library Long Write-up T604 (1982).

10) H. Goldstein, Classical mechanics, 2nd edition (Addison-Wesley, Reading, Mass.,
    1980), p. 147.

11) R.W. Hamming, Numerical methods for scientists and engineers (Mc Graw Hill,
    New York, 1962), p. 186.